UNITED NATIONS EDUCATIONAL, SCIENTIFIC AND CULTURAL ORGANIZATION
INTERNATIONAL ATOMIC ENERGY AGENCY
INTERNATIONAL CENTRE FOR THEORETICAL PHYSICS
I.C.T.P., P.O. BOX 586, 34100 TRIESTE, ITALY, CABLE: CENTRATOM TRIESTE

H4.SMR/916 - 10

SEVENTH COLLEGE ON BIOPHYSICS:

Structure and Function of Biopolymers: Experimental and Theoretical Techniques.

4 - 29 March 1996

Spectroscopy

R. SANCHES
Detp. Fisica e Informatica
Instituto de Fisica de Sao Carlos
Universidade de Sao Paulo
Brazil

Spectroscopy 1

Photoacoustic Spectroscopy and Applications in Biology

Rosemary Sanches
Dept. Física e Informática
Instituto de Física de São Carlos
Universidade de São Paulo
Brazil

Spectroscopy ⇒

Study of the interaction of light with matter

Matter ⇒ Characterized by energy levels

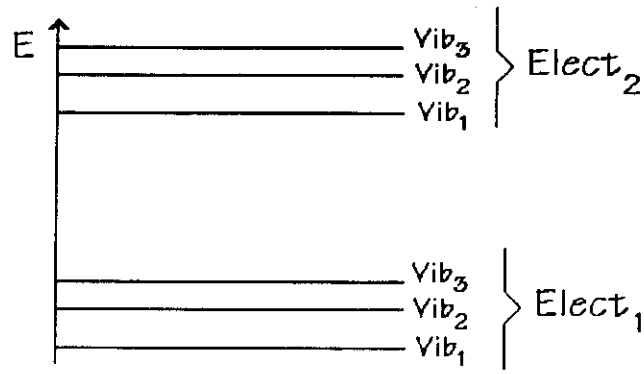

Transition

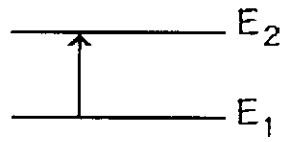

$E = E_2 - E_1$

How? With light

Light - Photon particles

Each photon → $E = \frac{hc}{\lambda}$

h: Planck const.
c: Velocity of light

UV-visible Light:
200 - 750 nm
⇓
electronic transitions

Infrared Light:
750 nm - 50 μm
⇓
vibrational transitions

Spectroscopic Techniques

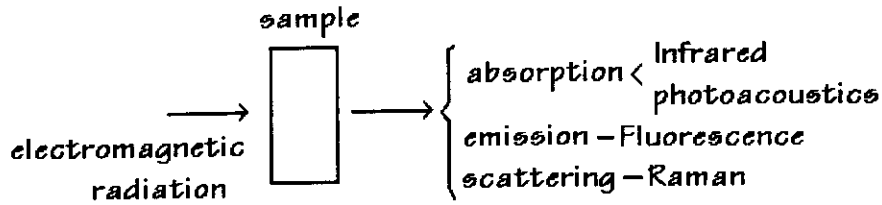

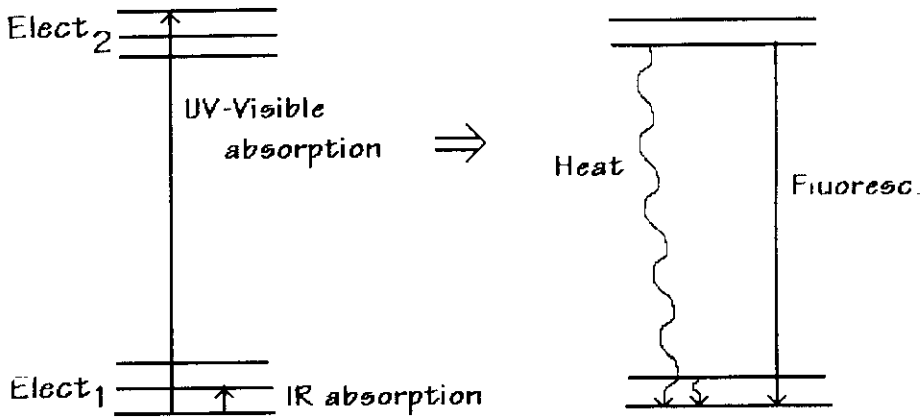

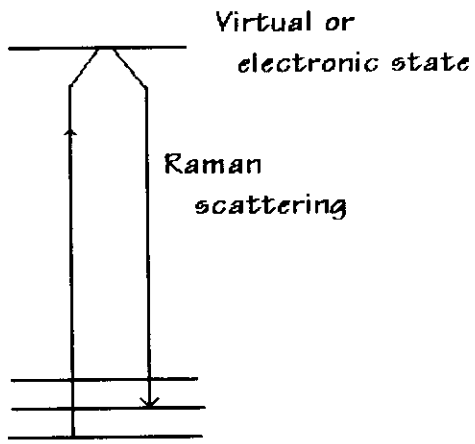

▷ Absorption Spectroscopy ⇒

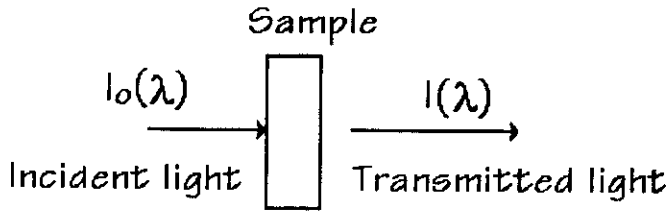

Absorbance:

$$A = \log(I_o/I)$$

Varying $\lambda \rightarrow$ Absorption spectrum

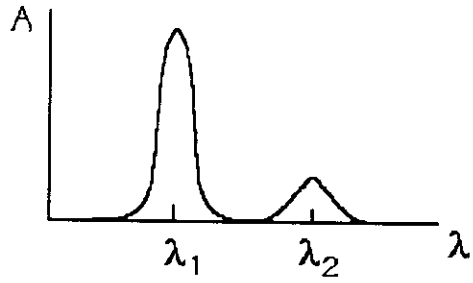

Therefore, Sample must be transparent !...

▷ Photoacoustic Spectroscopy

- Same kind of information $\begin{cases} UV - visible \rightarrow electr.transitions \\ infrared \rightarrow vibrat.transitions \end{cases}$
- Opaque samples

Photoacoustic Effect -

A.G. Bell, "The production of sound by radiant energy"
Phil. Mag. 11, 510 (1881)

Rosencwaig and Gersho, Applications to solids ('70s)

Photoacoustic Effect ⇒

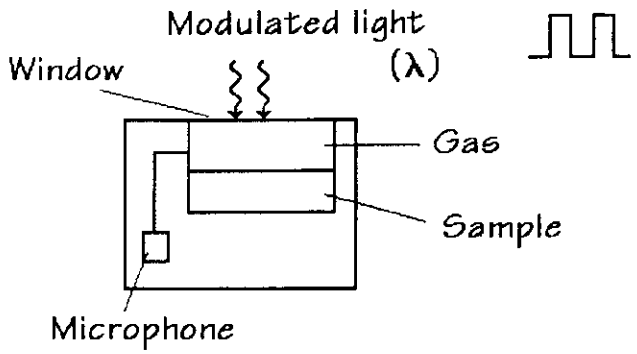

Photoacoustic Cell

Process:

Absorption of light by sample (λ)

↓

Sample is heated periodically

↓

Heat is transmitted to the gas

↓

Periodically oscilation of pressure

↓

Acoustic wave detected by microphone

More absorption ⇒ Larger signal from microphone

Varying λ ⇒ "Absorption Spectrum"

More.... Depth profile

Sample: 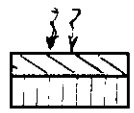

Phase lag between surface and inner signals

One dimensional Model

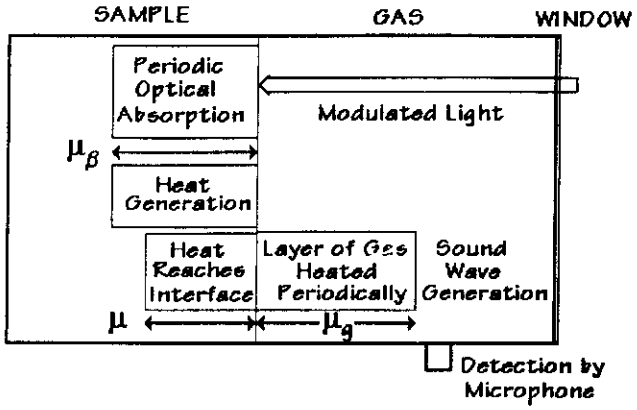

μ_β: Optical Absorption Length of Sample

μ : Thermal Diffusion Length of Sample

μ_g : Thermal Diffusion Length of Gas

❶ Modulated Incident light

$$I_{inc}(t) = \frac{I_0}{2}(1+\cos\omega.t)$$

$\omega = 2\pi f$ $\quad$ $f \approx 10$ Hz $\rightarrow$ 1 KHz

❷ Absorption

$$I(x) = I_{inc}\exp(-\beta x)$$

$\beta(\lambda)$: Absorption Coefficient $\quad \mu_\beta = \frac{1}{\beta}$

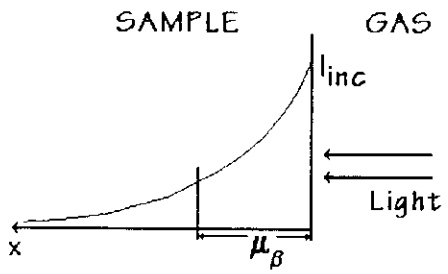

Light Absorbed: $I_{abs} = I_{inc} - I_{inc}e^{-\beta x}$

Light Absorbed in dx: $dI_{abs} = \beta I_{inc}e^{-\beta x}dx$

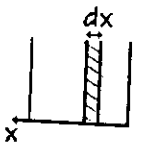

❸ De-excitation Paths

Processes:

- Fluorescence Decay
- Heat Generation ⟶ Contribute to PAS
- Photochemical Process ⟶ May contribute to PAS

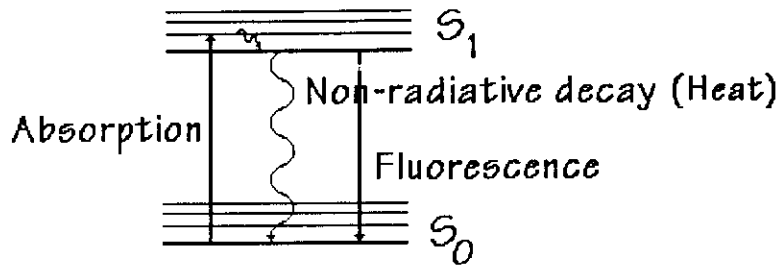

Heat generated in dx:

$$dH(x) = \eta\beta \frac{I_0}{2}(1+\cos\omega t)e^{-\beta x}dx$$

η: quantum yield for the conversion of the excitation energy into heat

❹ Heat conduction in the sample

Thermal diffusion equation: $\frac{\partial^2 T}{\partial x^2} = \frac{1}{\alpha}\frac{\partial T}{\partial t} - \frac{1}{\kappa}\frac{dH}{dx}$

where T: temperature of sample

κ: thermal conductivity of sample

α: thermal diffusivity of sample

$\alpha = \frac{\kappa}{\rho c}$ ρ: density of sample

c: specific heat of sample

Solution of thermal diffusion equation:

heat waves

$$T(x) = \begin{cases} Amplitude & \propto e^{-x/\mu} \\ Phase\ lag & \propto x/\mu \end{cases}$$

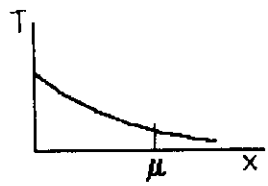

μ: thermal diffusion length

$$\mu = \sqrt{\frac{2\alpha}{\omega}}$$

VALUES OF THERMAL PARAMETERS FOR VARIOUS MATERIALS

Substance	Density ρ (g/cm^3)	Specific heat C (cal/g-°C)	Thermal Conductivity κ(cal/cm-sec-°C)	Thermal Diffusivity $\alpha = \kappa/\rho C$ (cm^2/sec)	Thermal diffusion Length at 100 Hz $\mu = (2\alpha/\omega)^{1/2}$(cm)
Aluminum	2.7	0.216	4.8×10^{-1}	0.82	5.1×10^{-2}
Stainless steel	7.5	0.12	3.3×10^{-2}	3.7×10^{-2}	1.1×10^{-2}
Brass	8.5	0.089	2.6×10^{-1}	0.34	3.3×10^{-2}
KCl crystal	2.0	0.21	2.2×10^{-2}	5.2×10^{-2}	1.3×10^{-2}
Crown glass	2.6	0.16	2.5×10^{-3}	6.0×10^{-3}	4.4×10^{-3}
Quartz	2.66	0.188	2.2×10^{-3}	4.4×10^{-3}	3.7×10^{-3}
Rubber	1.12	0.35	3.7×10^{-4}	9.4×10^{-4}	1.7×10^{-3}
Polyethylene	0.92	0.55	5×10^{-4}	9.9×10^{-4}	1.8×10^{-3}
Water	1.00	1.00	1.4×10^{-3}	1.4×10^{-3}	2.1×10^{-3}
Ethyl alcohol	0.79	0.60	4.2×10^{-4}	8.9×10^{-4}	1.7×10^{-3}
Chloroform	1.53	0.23	2.9×10^{-4}	8.4×10^{-4}	1.6×10^{-3}
Air	1.29×10^{-3}	0.24	5.7×10^{-5}	0.19	2.5×10^{-2}
Helium	1.80×10^{-4}	1.25	3.4×10^{-4}	1.52	7.0×10^{-2}

Source: Rosencwaig, 1978.

❺ Heat conduction in the gas

Thermal diffusion equation: $\frac{\partial^2 T_g}{\partial x^2} = \frac{1}{\alpha_g}\frac{\partial T_g}{\partial t}$

where T_g: temperature of gas

α_g: thermal diffusivity of gas

Boundary conditions at sample-gas interface:

- Temperature → $T_{(interf,t)} = T_{g(interf,t)}$
- Heat flux → $\kappa \frac{\partial T_{(interf,t)}}{\partial x} = \kappa_g \frac{\partial T_{g(interf,t)}}{\partial x}$

SOLUTION:

$T_g(x) \propto \exp(-x/\mu_g)$

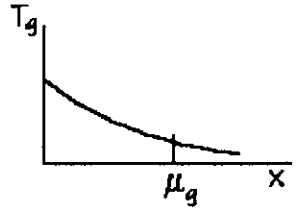

❻ Ideal Gas

$$\langle p_g(t) \rangle \propto \int_L T_g(x,t)\, dx \Rightarrow \textit{Mic. Signal}$$

Mic. Signal → Amplitude S

Phase shift ϕ

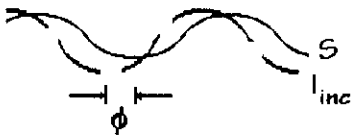

❼ PAS Signal

- $\mu < \mu_\beta \Rightarrow$ condition to have a spectroscopic tool

  $S_s(\lambda) \propto \beta(\lambda).I_o(\lambda)$

  ↖ Problem !

- $\mu > \mu_\beta \Rightarrow$ saturation (black body)

  $S_R(\lambda) \propto I_o(\lambda)$ (independent of β)

$$PAS = \frac{S_S}{S_R}$$

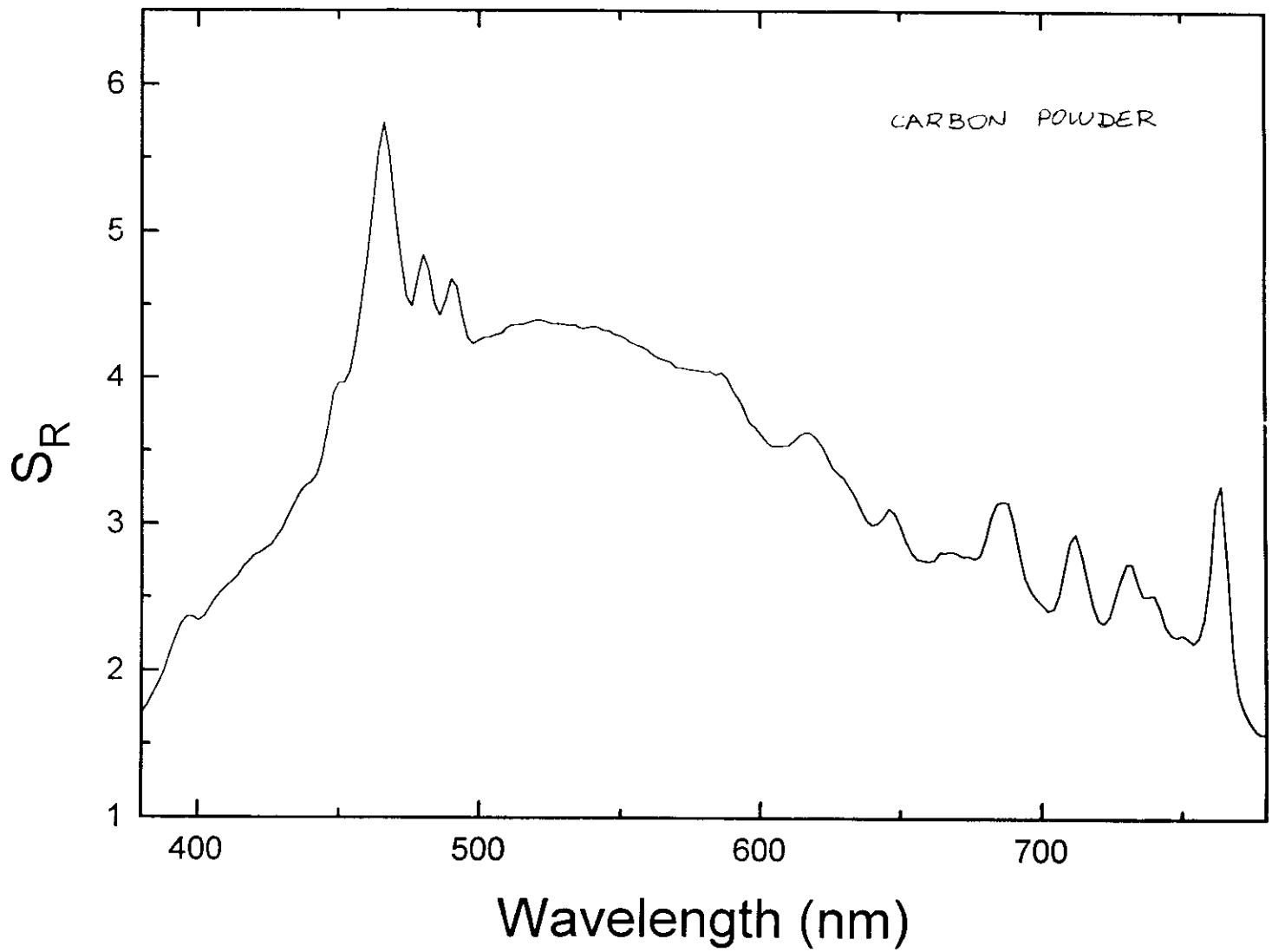
CARBON POWDER
S_R
6
5
4
3
2
1
400
500
600
700
Wavelength (nm)

Equipment

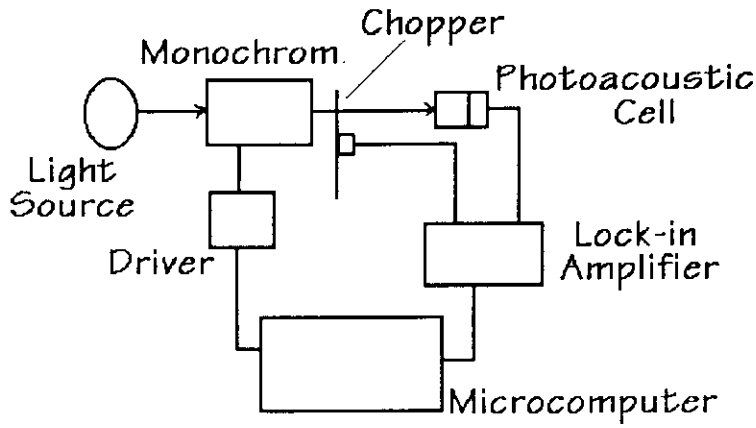

- Light Source: UV-Visible → Xe Lamp (400-1000 W)
  Lasers
  Infrared → Globar
- Monochromator → Holographic gratings
- Chopper →

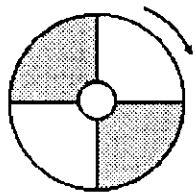

- Lock-in Amplifier → amplifies signal with the chopper frequency
- Photoacoustic Cell → detector:
  microphone
  pyroelectric material

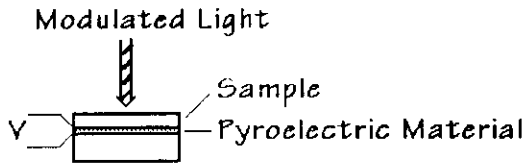

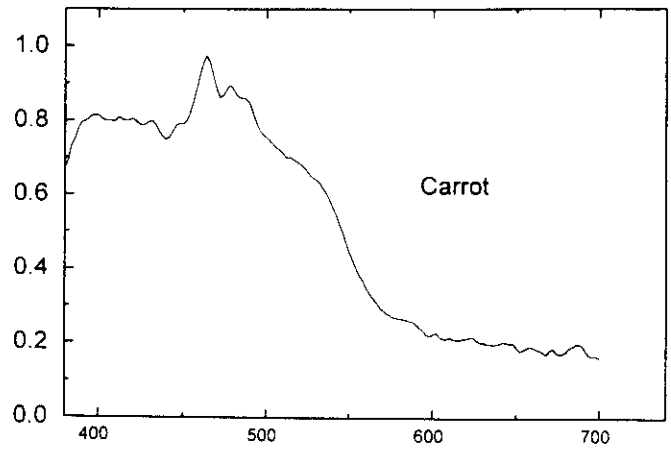

β-carotene

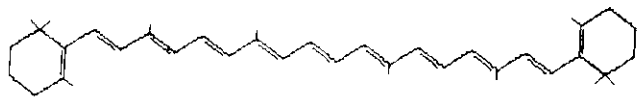

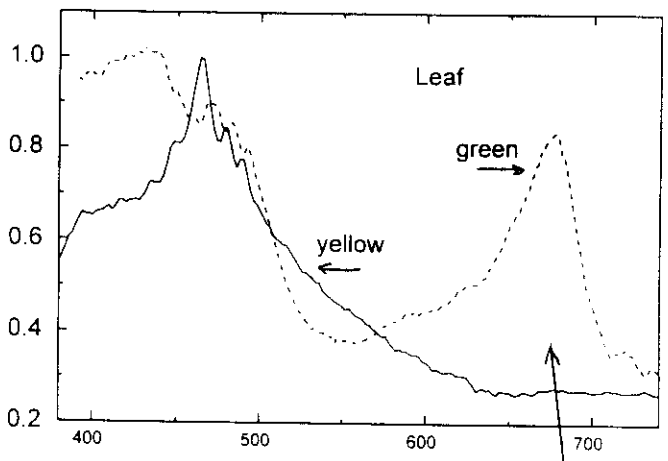

Chlorophyll

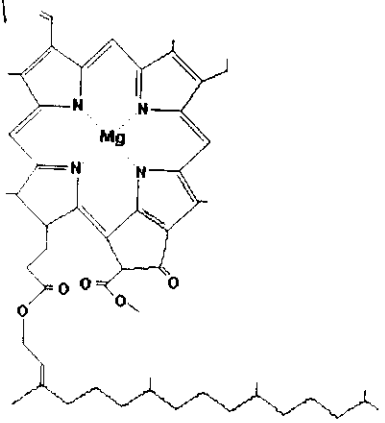

Depth Profile

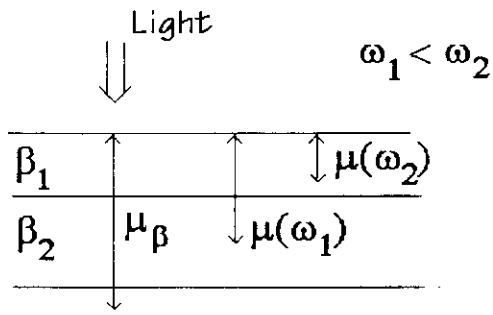

- Different modulation frequencies
  $\omega_1 \rightarrow$ upper + lower layers spectrum
  $\omega_2 \rightarrow$ upper layer spectrum

$$\mu = \sqrt{\frac{2K}{\omega \rho c}}$$

- Phase resolved measurements
  Delay of the interior signal from surface signal → phase lag

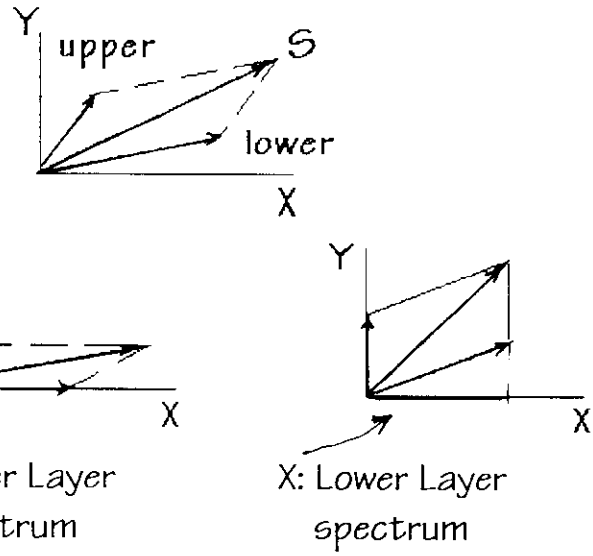

Depth Profile of β-carotene in Skin

D.M. Anjo and T.A. Moore

Photochem. Photobiol. 39, 635 (1984)

Mouse fed with β-carotene ⇒ Skin from ear

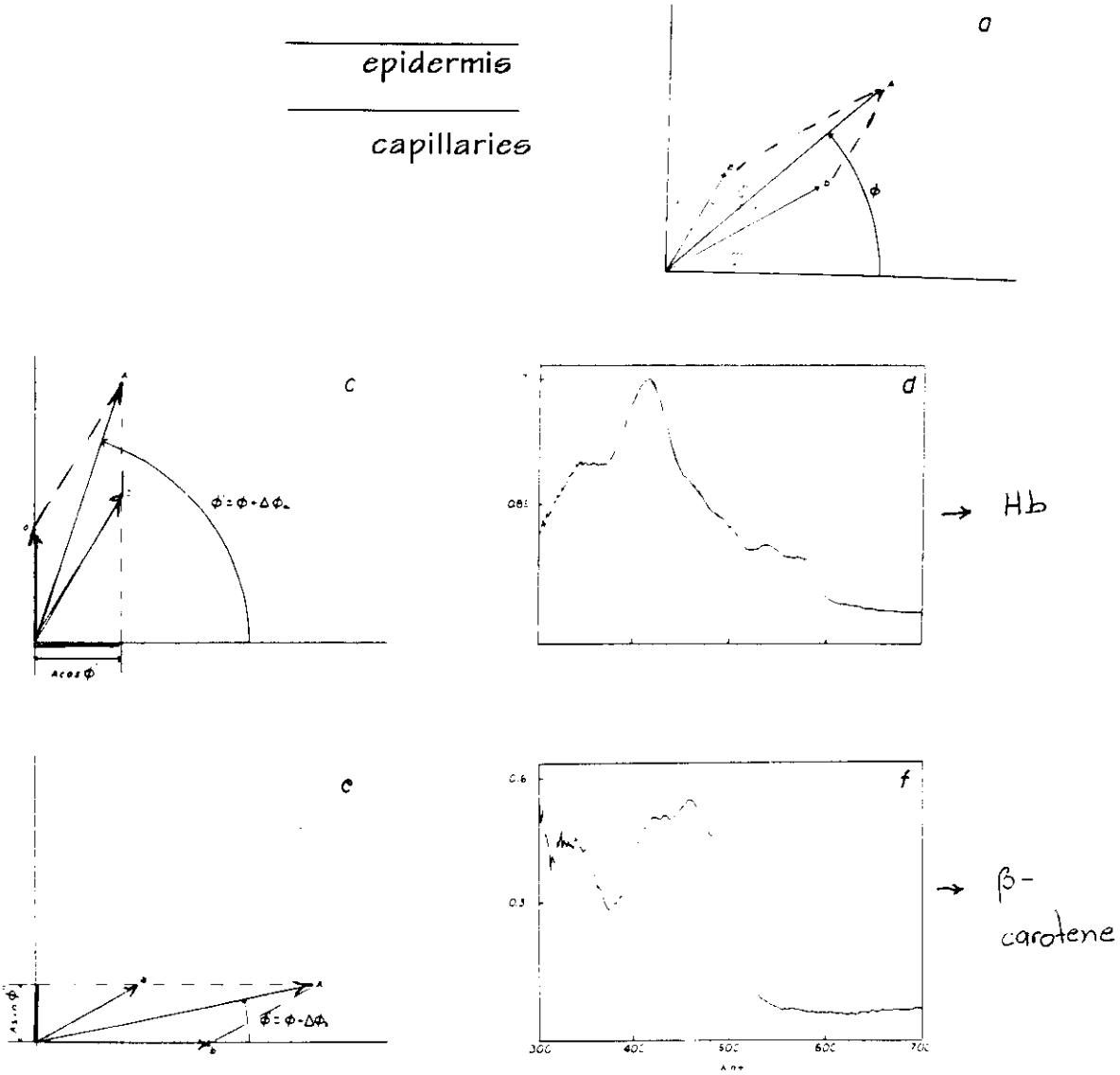

Figure 3. (a) Two vector model of PAS response at one discrete wavelength. surface vector is **a** and interior vector is **b** absolute magnitude is *A*. (b) Phase (- - -) and magnitude (—) spectra of the poly (methylmethacrylate) model recorded at 150 Hz. (c) The phase lead is increased until vector **a** is eliminated from the cosine projection, generating a pure interior signal. (d) The phase separated interior spectrum of the model showing the hemoglobin spectrum. (e) The phase lead is decreased until the **b** component is eliminated from the sine projection, generating a pure surface signal. (f) The phase separated spectrum of the surface component β-carotene

Penetration of Sunscreen into Human Skin

K. Giese, A. Nicolaus, B. Sennhenn and K. Kölmel

Can. J. Phys. 64, 1139 (1986)

In vivo measurements ⇒ Open-ended cell

Sunscreen applied to the skin of the forearm (inner part)

Forearm pressed to the cell rim

In stratum corneum ⇒ μ= 10 μm at 180 Hz

4 μm at 1200 Hz

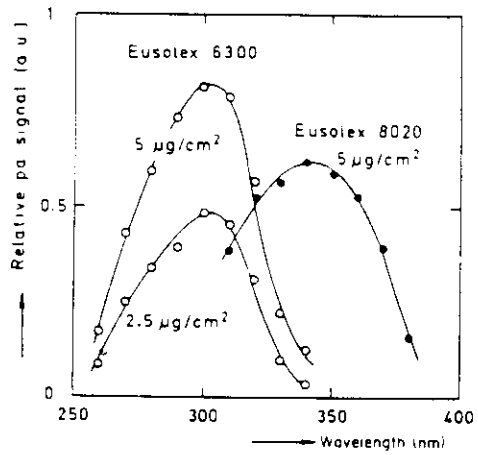

Fig. 4 Photoacoustic (pa) absorption spectra of Eusolex 6300 and Eusolex 8020, measured in vivo at a chopping frequency of 1200 Hz. The differences between the signals of treated and untreated skin are plotted

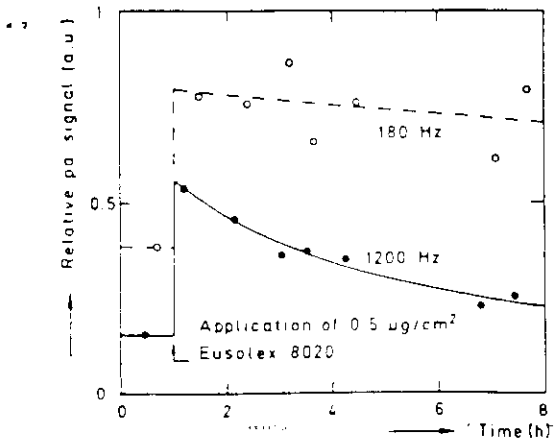

Fig. 3. Time dependence of the photoacoustic (pa) in vivo signal of stratum corneum after topical application of Eusolex 8020 in isopropanolic solution (wavelength = 350 nm; a.u.—arbitrary units).

Sunscreen penetrates stratum corneum.

References

A. Rosencwaig. *Photoacoustics and Photoacoustic Spectrosocopy*, John Wiley & Sons, New York (1980)

T.A. Moore. *Photoacoustic Spectroscopy and Related Techniques Applied to Biological Materials*,Photochem. Photobiol. 7, 187 (1983)

A.C. Tam. *Applications of Photoacoustic Sensing Techniques*, Rev. Mod. Phys. 58, 381 (1986)

S.E.Braslavsky. *Photoacousitc and Photothermal Methods Applied to the Study od Radiationless Deactivation Processes in Biological Systems and in Substances of Biological Interest*, Photochem. Photobiol. 43, 667 (1986)

K.S. Peters, T. Watson and K. Marr. *Time-resolved Photoacoustic Calorimetry: a Study of Myoglobin and Rhodopsin*, Annu. Rev. Biophys. Biophys. Chem. 20, 343 (1991)

Spectroscopy 2

Infrared Spectroscopy and Applications in Biology

Rosemary Sanches
Dept. Física e Informática
Instituto de Física de São Carlos
Universidade de São Paulo
Brazil

Infrared Absorption Spectroscopy

Applications:

Protein - Secondary structure determination

Nucleic Acids - Overall structure and interaction with small molecules (intercalating drugs or metal ions)

Lipids in Membranes - Phase transitions

Dynamics of reactions - time-resolved spectroscopy

Difficulty for Biological Samples:

Strong absorption of water molecules

Improvements:

FT-IR ⇒

based on the Michelson interferometer

fast Fourier transform algorithm

Mathematical Calculations ⇒

- spectral subtraction of the water bands
- deconvolution or derivation of the spectrum
- curve fitting

} To resolve the multicomponent bands

Sampling Techniques ⇒

- transmission
- attenuated total reflectance (ATR)
- IR microscopy
- linear dichroism

▷ Dispersive Instrument ⇒

Absorbance: $A = \log(I_o/I)$

▷ FT-IR Instrument ⇒

Michelson Interferometer -

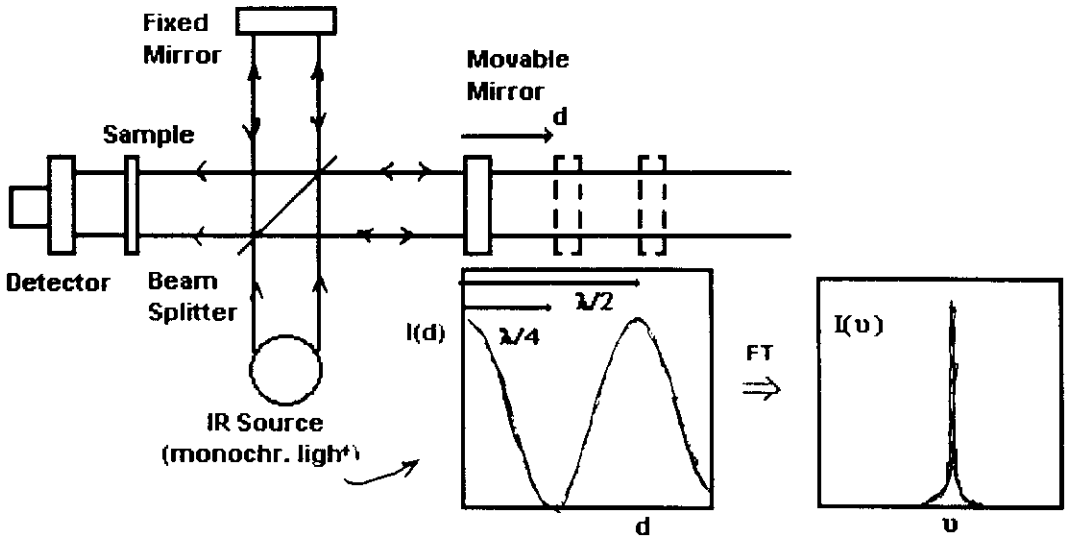

$$I(d) = I \cos(4\pi d/\lambda)$$

$\delta = 2d$: difference in path length

$\nu = 1/\lambda$

$$I(\delta) = I \cos(2\pi\delta\nu)$$

For a polychromatic source:

$$I(\delta) = \int_{-\infty}^{+\infty} I(\upsilon)\, \cos(2\pi\upsilon\delta)\, d\upsilon$$

$$I(\delta) \overset{FT}{\Rightarrow} I(\nu)$$

$$I(\upsilon) = \int_{-\infty}^{+\infty} I(\delta)\, \cos(2\pi\upsilon\delta)\, d\delta$$

Get $I(\nu)$ and get $I_o(\nu) \rightarrow$ Obtain I_o/I

Absorbance: $A = \log(I_o/I)$

Resolution - determined by the distance the mirror moves (d)

Truncation of the integral

▷ **Advantages of FT-IR**

- No need to scan → greater S/N ratio in the same acquisition time
- No need of slits (defined resolution)
- Better frequency calibration (internal laser reference is used)

▷ Sampling Techniques

- Cells, windows, pellets

  Material: CaF_2, BaF_2, ZnSe, IRTRAN, KBr, AgCl

  For solutions in water → very thin cells ($\leq 10\,\mu m$)

- Attenuated Total Reflectance (ATR)

  Good for films

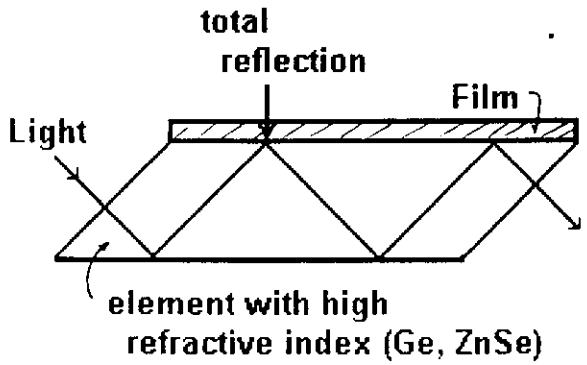

  (used to study membranes)

- IR microscopy

  Good for crystals

- Linear dichroism

  Good for oriented samples

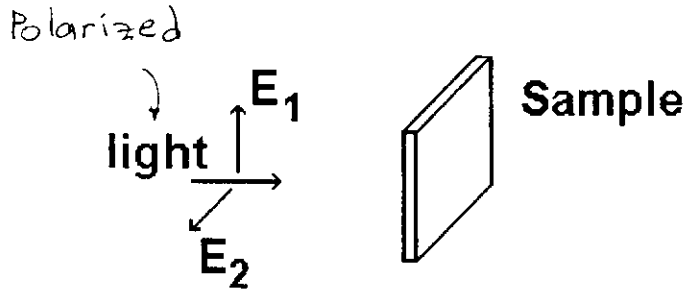

(used to study orientation of helix in membrane-associated proteins)

▷ Theoretical Background ⇒

IR spectroscopy → vibrational frequencies

CLASSICAL DESCRIPTION:

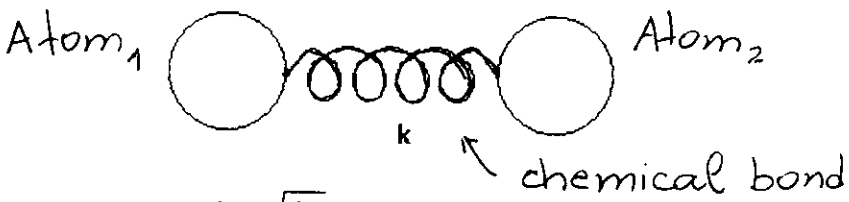

$$f = \frac{1}{2\pi}\sqrt{\frac{k}{\mu}}$$

μ: reduced mass

QUANTUM MECHANICAL:

Selection rules:

1) Vibrational transitions -

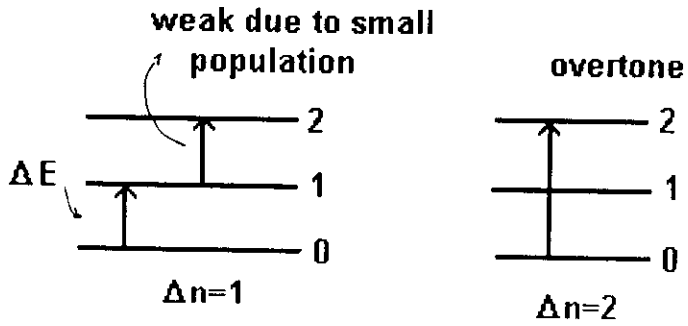

2) Dipole moment must change during vibration

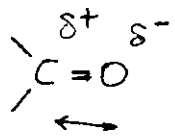

Classification of vibrations ⇒

- Stretching → involves changes in bond lengths
- Bending → involves changes in bond angles

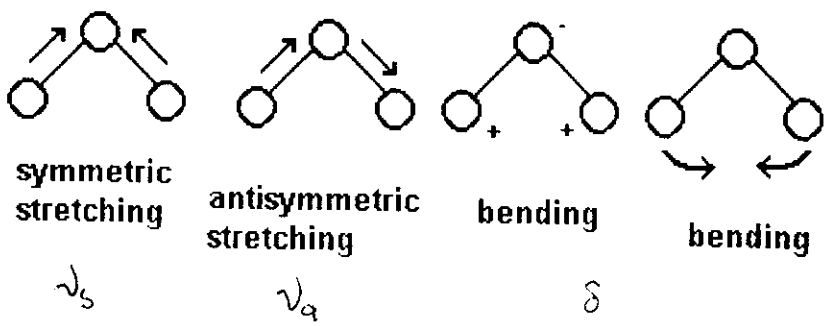

Group Frequencies ⇒

frequencies characteristic of chemical groups

Example: $-CH_2-$ → $\nu_s \approx 2850\ cm^{-1}$

However → group frequencies are affected by inter or intra-molecular interactions

Example, in proteins $\rangle C{=}O \cdots H{-}N\langle$

ν_s { α-helix, β-sheet

Band Assignment ⇒

- **Normal Mode Analysis:**

  Biological Molecules → too complex

- **Problem of Aqueous Solutions:**

	H_2O	D_2O	
ν_s	3920 cm^{-1} (sh)	2900 cm^{-1} (sh)	
	3490	2540	Too strong Saturates detector
	3280	2450	
ν_a	2125	1555	
δ	1645	1215	

J.R.L. Arrondo et al. (1993)

For proteins → Use thin samples in H_2O or use D_2O

▷PROTEINS ⇒

Peptide Bond:

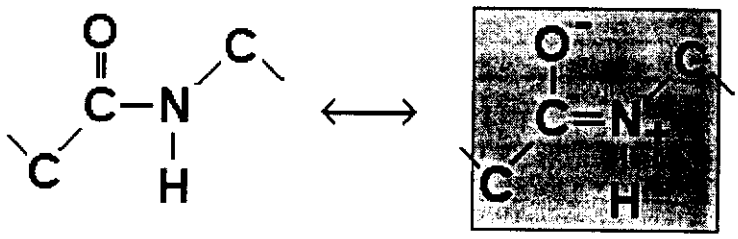

Amide group vibrations →

In plane: $\nu_{C=O}$, ν_{C-N}, ν_{N-H}, δ_{OCN}, δ_{CNH}

Out of plane: τ_{C-N}, $\delta_{C=O}$, δ_{N-H}

Model System → N-methylacetamide
(normal mode calculations)

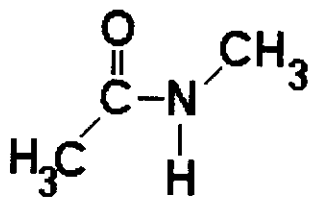

	observed cm^{-1}	
Amide A	3236 (S)	ν_{N-H} (100%)
+Amide B		
Amide I	1653 (S)	$\nu_{C=O}$ (83%) + ν_{C-N} + δ_{CCN}
II	1567 (S)	δ_{CNH} (49%) + ν_{C-N} (33%) + δ_{OCN} + ν_{C-C} + ν_{C-N}
III	1299 (M)	δ_{CNH} (52%) + ν_{C-N} (14%) + ν_{C-C} + δ_{OCN}
V	725 (S)	δ_{NH} + τ_{C-N}
VI	600 (M)	$\delta_{C=O}$ + τ_{C-N}

J. Bandekar (1992)

Assignment of Bands to Secondary Structure

Guided by: theoretical calculations and
spectra-structure correlations for peptides and proteins of known structure

Most of the work uses the Amide I band (sometimes also de Amide II)

Homopolypeptides → often purely α-helical or β-sheet or unordered

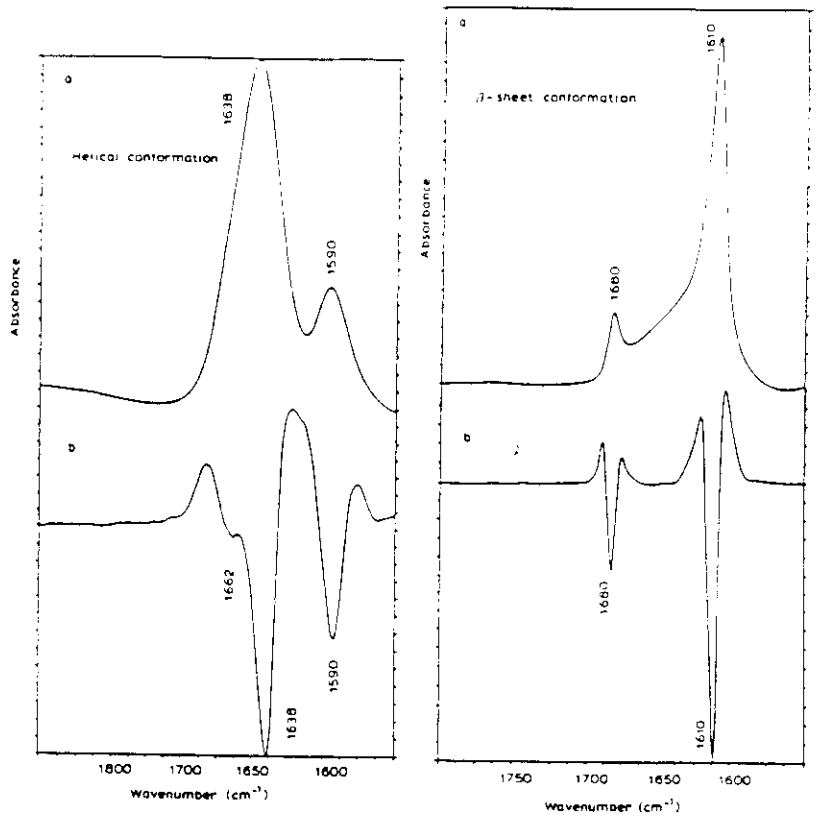

FIGURE 1 FTIR absorbance (a) and second-derivative (b) spectra of poly-L-lysine in aqueous solution (^2H_2O) recorded in its α-helical and β-sheet conformations. The spectra were recorded at 20°C.

P.I. Haris & D. Chapman (1995)

Amide I frequency for different secondary structures → polypeptides ≠ proteins

Proteins → mixture of different amino acids → different strength of hydrogen bonding within the secondary structures

TABLE II

Deconvolved Amide I Frequencies and Assignments (cm^{-1})

Protein	Extended Chains			High Components	Helix	Unordered	Turns and Bends				
	Low Components										
Carbonic anhydrase	1636		1625	1678	1653	1645	1660	1668		1690	
Carboxypeptidase	1635	1628	1623	1679	1652	1642	1665	1671		1690	
Casein						1644		1671			
α-Chymotrypsin	1637		1627	1674	1654	1647	1665		1681	1688	
Chymotrypsinogen	1637		1627	1674	1654	1646	1664		1682	1688	1696
Concanavalin A	1639	1634	1623	1671	1653	1646	1659		1684		1694
Elastase	1639	1633	1620	1673	1657	1645	1665		1683		
Immunoglobulin G	1637		1624	1672	1651		1659			1688	
α-Lactalbumin	1637		1627	1676	1652	1644	1665		1684		
β-Lactoglobulin		1634	1623	1679	1654	1646	1665		1685		1692
Lysozyme		1630		1673	1654	1641	1666		1682		
Papain	1640	1632	1621	1679	1654	1646	1662	1670		1687	
Ribonuclease A	1637	1628		1676	1655	1646	1665		1684	1688	
Ribonuclease S		1633		1672	1653	1645	1663		1681		
Trypsin	1638		1627	1673	1654	1646	1664		1681		
Trypsinogen	1636		1624	1675	1654	1646	1663		1684		1693
Trypsin inhibitor (soybean)	1636			1675	1656	1646	1664		1685		
Rounded Average	1637	1631	1624	1675	1654	1645	1663	1670	1683	1688	1694
RMS Deviation	1.4	2.5	2.4	2.6	1.5	1.6	2.2	1.4	1.5	1.1	1.7
Maximum Absolute Deviation	3	3	4	4	3	4	4	2	2	2	2

D.M. Byler & H. Susi (1986)

- Protein Structure and Amide I Frequenc

Structure	cm^{-1}
antiparallel β-sheet or aggregated strands	1675-1695
3_{10}-helix	1660-167C
α-helix	1648-166C
unordered	1640-164E
β-sheet	1625-164C
aggregated strands	1610-162E

M. Jackson & H.H. Mantsch (1995)

Caution in Assignment →

Myoglobin - predominantly α-helical

IR spectrum - Amide I maximum at 16E

shoulder at 1632 cm^{-1} —

Most probably turns

Protein → mixture of different secondary s

Amide I: overlapping bands from differen

Data Processing ⇒

▷ Difference Spectroscopy

$$S_d = S_A - k\,S_B$$

- Subtraction of water spectrum (or buffer)

water bands: remove band at 2125 cm^{-1}

flat baseline 1900-1720 cm^{-1}

deuterium bands: remove band at 1220 cm^{-1}

flat baseline 2100-1730 cm^{-1}

- Study of small changes in conformation of biological molecules

▷ Fourier Deconvolution

To resolve the multicomponent Amide I band

Profile of IR band → Lorentzian function

$$A(\nu) = A_0 \frac{\gamma^2}{\gamma^2 + (\upsilon - \upsilon_0)^2}$$

↓ Cos Fourier transform

$$I(x) = \mathcal{F}[A(\upsilon)] = \int_0^\infty A(\upsilon)\cos(2\pi\upsilon x)\,d\upsilon = \frac{A_0\gamma}{2}\cos(2\pi\upsilon_0 x)e^{-2\pi\gamma x}$$

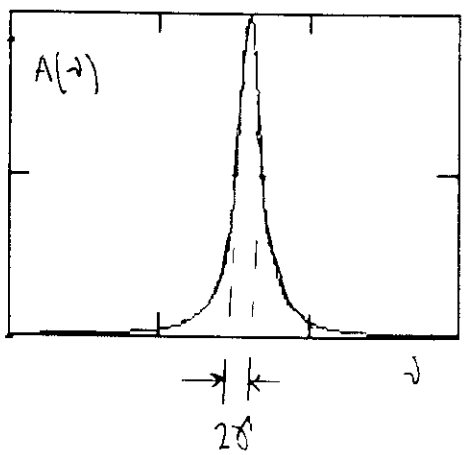

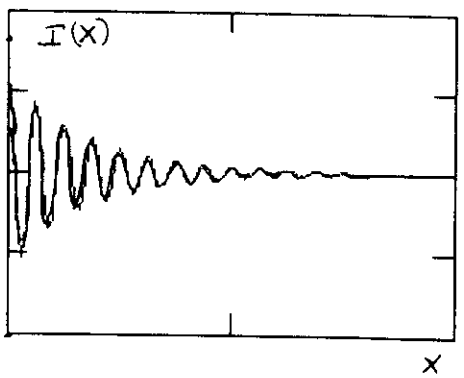

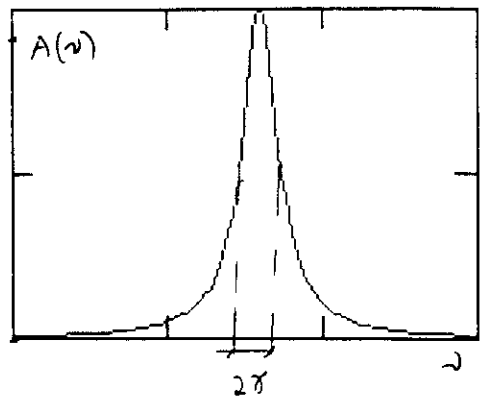

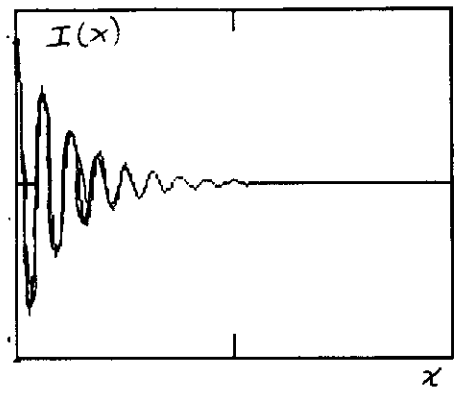

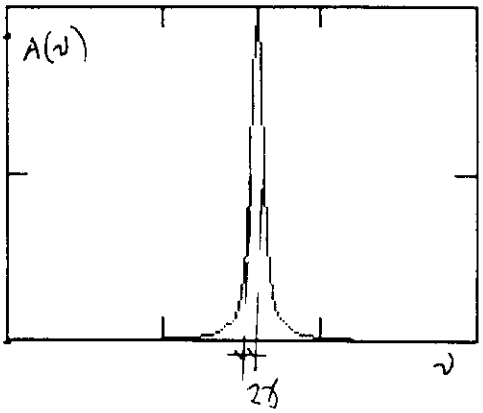

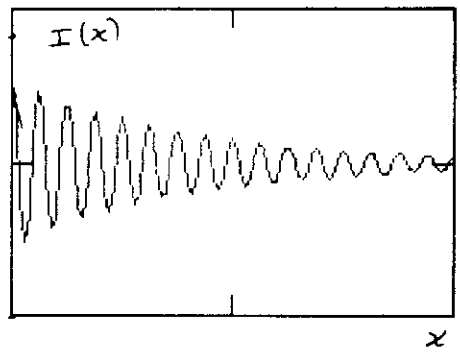

In Practice $\Rightarrow$

Get absorbance spectrum: A(ν)

$$I(x) = \mathcal{F}[A(\upsilon)]$$

$$I'(x) = I(x)e^{2\pi\gamma x}D(x)$$ γ has to be estimated

truncation

$$\mathcal{F}^{-1}\{I'(x)\} = A'(\upsilon)$$ ← Narrower Bands

One gets - number of bands and their position

Problem - degradation of S/N ratio

▷ Derivative
(2nd or 4th)

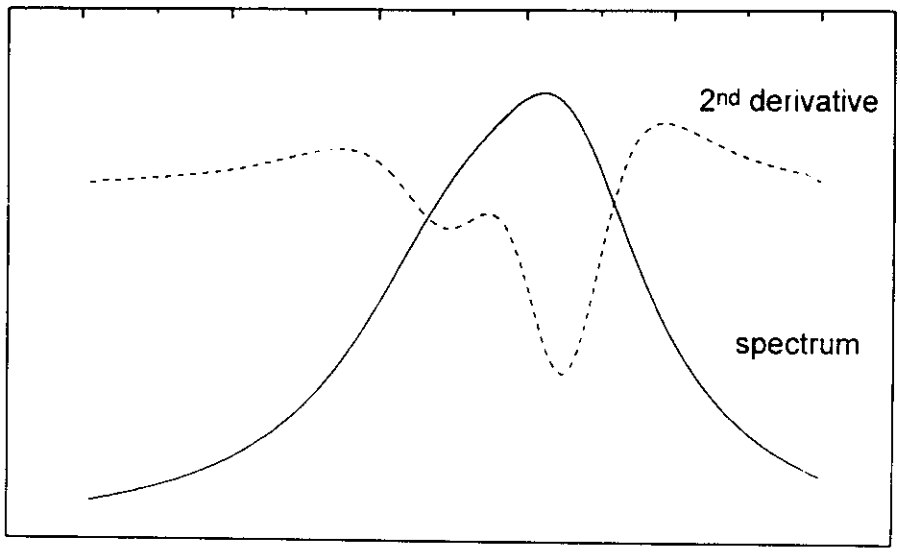

One obtains: number of bands and their position

Problem → degradation of S/N ratio

Quantifying the Secondary Structures

▷ Curve Fitting
- Fit Lorentzian (or Gaussian) bands to original spectrum or to deconvolved spectrum
  Position and number of bands → given by derivative or deconvolution
  Adjust height and width
- Correlate position of bands to different secondary structures
- Amounts of different structures → from area under the bands (Assumption: same molar absorptivity for the different bands!!!)

IR Spectra of Proteins in Solution and Crystalline Forms

J.M. Hadden, D. Chapman & D.C. Lee

Biochim. Biophys. Acta 1248, 115 (1995)

For solution:

Conc.: 30 mg protein/ml in phosphate buffer (pH 7.0)

$\ell = 6\ \mu m$

For crystals:

Area: from 10 μm x 10 μm to 50 μm x 50 μm

Kept in presence of mother liquor

Hen Egg White Lysozyme

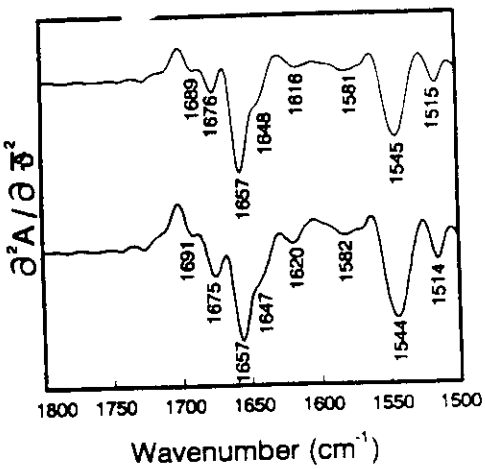

Fig. 2. Second-derivative infrared spectra recorded from a solution (top trace) and a single crystal (bottom trace) of hen egg white lysozyme.

Solution and crystal structures are very similar (predominance of α-helix)

Bovine Pancreatic Ribonuclease A

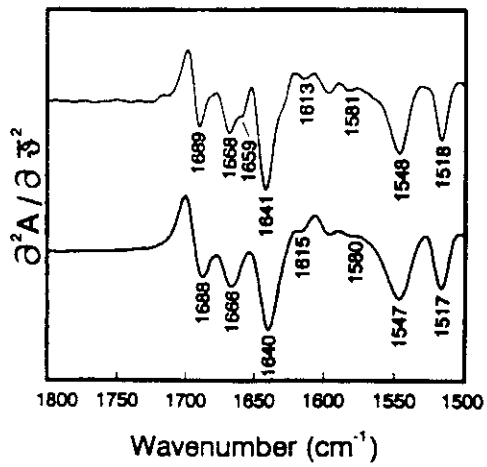

Fig. 3. Second-derivative infrared spectra recorded from a solution (top trace) and a single crystal (bottom trace) of bovine pancreatic ribonuclease A.

Small difference ≈ 1659 cm^{-1}

Structures are similar (predominance of β-sheet)

Table 2

Protein	Crystal (cm^{-1})						Solution (cm^{-1})					
	Absorbance spectra		Second-derivative spectra				Difference spectra		Second-derivative spectra			
	Am I	Am II	β-sheet	turns	α-helix/random	β-sheet	Am I	Am II	β-sheet	turns	α-helix/random	β-sheet
LYS	1656	1545	1691	1675	1657	–	1657	1545	1689	1676	1657	–
RNa	1642	1547	1688	1666	–	1640	1641	1548	1689	1668	1659	1641
GC	1642	1549	1688	–	1633 (3_{10})?	1633	1638	1547	1685	–	1661 (3_{10})?	1633
SAPC	1640	1557	1688	1668	1652	1636	1635	1550	1687	–	1655	1634
END	1650	1545	1688	–	1663 (3_{10})?	1637	1641	1548	1690	1673	1663 (3_{10})?	1640
MUC	1646	1544	1685	–	1661 (3_{10})?	1641	1643	1529	1688	1676	1658	1642

Band assignments in protein solution and crystal spectra.

Serum Amyloid P Component

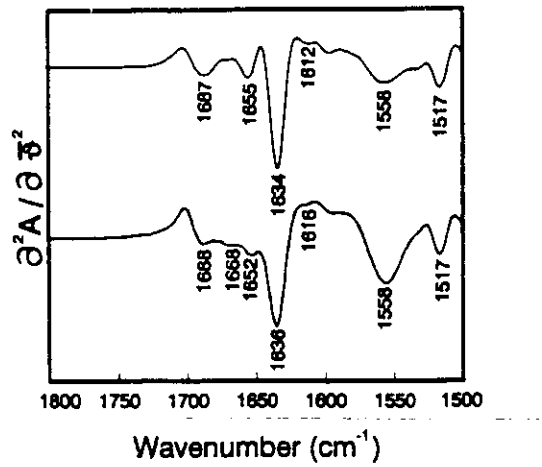

Fig. 5. Second-derivative infrared spectra recorded from a solution (top trace) and a single crystal (bottom trace) of human serum amyloid P component.

Differences: ≈ 1668 cm^{-1} (turns)
reduced α-helical content in crystal
(predominance of β-sheet)

Endothia Parasitica Pepsin

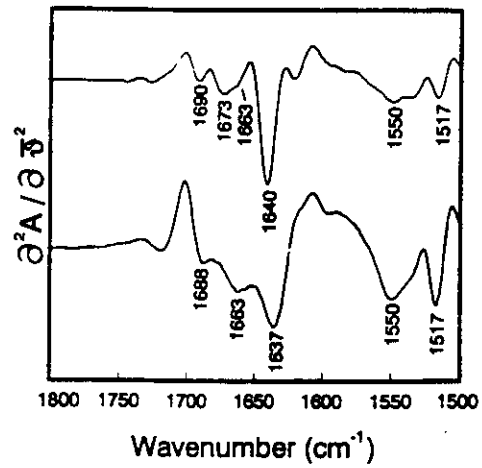

Fig. 6. Second-derivative infrared spectra recorded from a solution (top trace) and a single crystal (bottom trace) of *Endothia parasitica* pepsin.

Small difference ≈ 1673 cm^{-1}
(turns)

(predominance of β-sheet)

References

General

1) Haris & D. Chapman, *Does Fourier-Transform Infrared Spectroscopy Provide Useful Information on Protein Structure?*, Trend Biochem. Sci. 17, 328 (1992)
2) J.L.R. Arrondo, A. Muga, J. Castresana & F.M. Goñi, *Quantitative Studies of the Structure of Proteins in Solution by Fourier-Transform Infrared Spectroscopy*, Prog. Biophys. Molec. Biol. 59, 23 (1993)
3) W.K. Surewicz, H.H. Mantsch & D. Chapman, *Determination of Protein Secondary Structure by FT-IR Spectroscopy: a Critical Assessment*, Biochemistry 32, 389 (1993)
4) F. Siebert, *Infrared Spectroscopy Applied to Biochemical and Biological Problems*, Methods Enzymology 246, 501 (1995)
5) M. Jackson & H.H. Mantsch, *The Use and Misuse of FTIR Spectroscopy in the Determinationof protein Structure*, Crit. Rev. Biochem. Molec. Biol. 30, 95 (1995)
6) P.I. Haris & D. Chapman, *The Conformational Analysis of Peptides Using Fourier Transform IR Spectroscopy*, Biopolymers 37, 251 (1995)

Mathematical Methods

• Water Subtraction

7) Dousseau, M. Therrien & M. Pézolet, *On the Spectral Subtraction of Water from the FT-IR Spectra of Aqueous Solutions of Proteins*, Appl. Spectr. 43, 538 (1989)

• **Derivative**

8) D.G. Cameron & D.J. Moffatt, *A Generalized Approach to Derivative Spectroscopy*, Appl. Spectr. 41, 539 (1987)

• **Deconvolution**

9) J.K. Kauppinen, D.J. Moffatt, H.H. Mantsch & D.G. Cameron, *Fourier Self-Deconvolution: a Method for Resolving Intrinsically Overlapped Bands*, Appl. Spectr. 35, 271 (1981)

10) W.J. Yang, P.R. Griffiths, D.M. Byler & H. Susi, *Protein Conformation by Infrard Spectroscopy: Resolution Enhancement by Fourier Self-Deconvolution*, Appl. Spectr. 39, 282 (1985)

11) D.M. Byler & H. Susi, *Examination of the Secondary Structure of Proteins by Deconvolved FTIR Spectra*, Biopolymers 25, 469 (1986)

• **Data Base Analysis**

12) F. Dousseau & M. Pézolet, *Determination of the Secondary Structure Content of Proteins in Aqueous Solutions from their Amide I and Amide II Infrared Bands. Comparison Between Classical and Partial Least-Squares Methods*, Biochemistry 29, 8771 (1990)

13) D.C. Lee, P.I. Haris, D. Chapman & R.C. Mitchell, *Determination of Protein Secondary Structure Using Factor Analysis of Infrared Spectra*, Biochemistry 29, 9185 (1990)

14) R.W. Sarver Jr. & W.C. Krueger, *Protein Secondary Structure from Fourier Transform Infrared Spectroscopy: a Data Base Analysis*, Anal. Biochem. 194, 89 (1991)

Difference Spectroscopy

15) W. Mäntele, *Reaction-Induced Infrared Difference Spectroscopy for the Study of Protein Function and Reaction Mechanisms*, Trends Biochem. Sci. 18, 197 (1993)

ATR Spectroscopy

16) Jackson & H.H. Mantsch, *Artifacts Associated with the Determination of Protein Secondary Structure by ATR-IR Spectroscopy*, Appl. Spectr. 46, 699 (1992)

Normal Mode Analysis

17) J. Bandekar, *Amide Modes and Protein Conformation*, Biochim.Biophys. Acta 1120, 123 (1992)

Spectroscopy 3

Raman Spectroscopy and Applications in Biology

Rosemary Sanches
Dept. Física e Informática
Instituto de Física de São Carlos
Universidade de São Paulo
Brazil

Raman Spectroscopy

Applications:

Protein and Nucleic Acids

- Conformational analysis
- Probe specific reaction sites
- Dynamics of biological processes (time-resolved mode)

Limitation:

Interference from fluorescence

However:

Good for aqueous samples (Raman scattering of water is very weak)

Improvements:

FT-Raman

New lasers (in special in the UV) and new detectors

Mathematical Calculations ⇒

- deconvolution or derivation of the spectrum
- curve fitting

} To resolve the multicomponent bands

The Raman Effect:

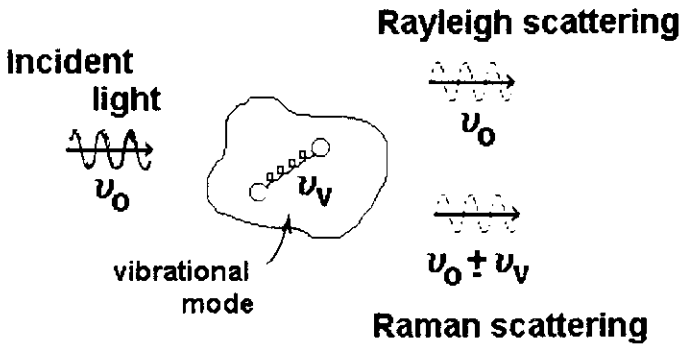

▷ No vibration of molecule ⇒

Electron cloud oscillation induced by exciting electromagnetic field → oscillating dipole moment is created:

$$\vec{\mu} = \alpha \vec{E} \qquad \alpha: \text{polarizability}$$

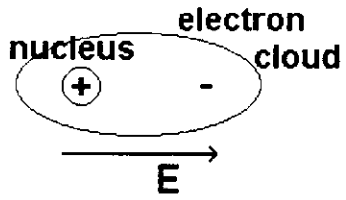

Charge is accelerating → radiation of electromagnetic waves with frequency υ_0 → elastic or Rayleigh scattering

▷ With vibration of molecule ⇒

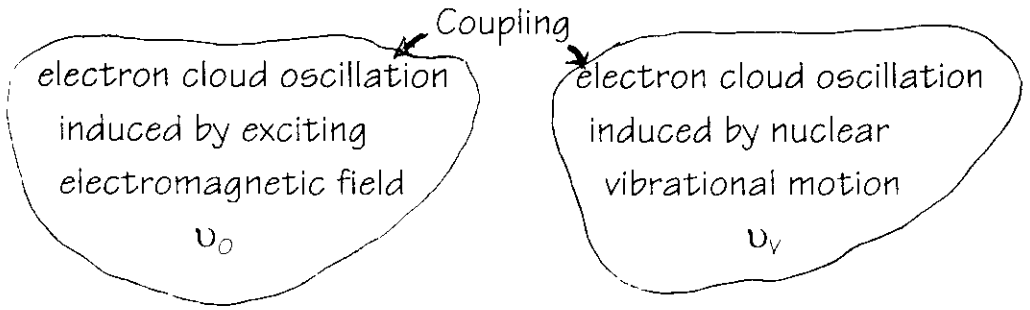

Coupling of the two oscillations → beat oscillations at $\upsilon_0 \pm \upsilon_V$

→ radiation of electromagnetic waves with frequencies $\upsilon_0 + \upsilon_V$ and $\upsilon_0 - \upsilon_V$ → inelastic or Raman scattering

Raman Scattering Intensity:

$$I_S \propto \upsilon_S^4 I_0 (\Delta\alpha)^2$$

υ_S: frequency of scattered light

I_0: intensity of incident light

$\Delta\alpha$: change in polarizability induced by the vibrational transition

Change in Polarizability

CLASSICAL FRAMEWORK $\Rightarrow$

- Electric field of incident light:

$$E = E_0 \cos(2\pi\upsilon_0 t)$$

- Interaction of E with molecule $\rightarrow$ induced dipole moment

$$\mu(t) = \alpha(q)E$$

q: nuclear coordenate $\rightarrow$ $q = A\cos(2\pi\upsilon_V t + \delta)$

- Polarizability must change with vibration !!!

$\alpha(q)$: expansion in a Taylor series

$$\alpha(q) = \alpha_0 + \left(\frac{\partial\alpha}{\partial q}\right)_0 q + \cdots$$

Therefore:

$$\mu(t) = \left[\alpha_0 + \left(\frac{\partial\alpha}{\partial q}\right)_0 A\cos(2\pi\upsilon_V t + \delta)\right] E_0 \cos(2\pi\upsilon_0 t)$$

$$= \underbrace{\alpha_0 E_0 \cos(2\pi\upsilon_0 t)}_{\text{Rayleigh}} + \frac{1}{2}\left(\frac{\partial\alpha}{\partial q}\right)_0 \underbrace{E_0 A\cos\left[2\pi(\upsilon_0 - \upsilon_V)t + \delta\right]}_{\text{Raman}} +$$

$$+ \frac{1}{2}\left(\frac{\partial\alpha}{\partial q}\right)_0 \underbrace{E_0 A\cos\left[2\pi(\upsilon_0 + \upsilon_V)t + \delta\right]}_{\text{Raman}}$$

If vibration doesn't change polarizability $\rightarrow$ no Raman effect

QUANTUM MECHANICAL VIEW

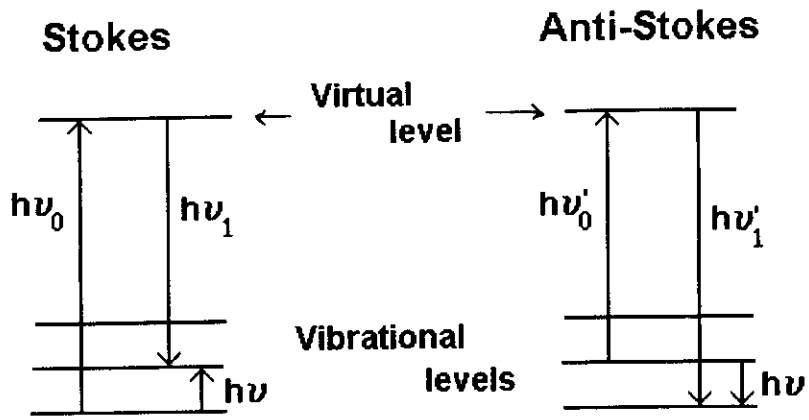

$h\nu = h\nu_o - h\nu_1$ → get ν

$h\nu = h\nu_1' - h\nu_o'$ → get ν

$$I_{anti\text{-}Stokes} << I_{Stokes}$$

Population of vibrational energy levels:

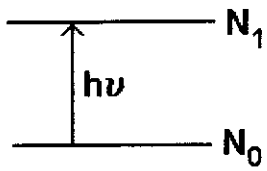

Boltzmann distribution:

$$N_1 = N_0 e^{-h\upsilon / kT} \qquad h\upsilon = hc\bar{\upsilon}$$

$\bar{\upsilon}$: wavenumber

At 300 K and for $\bar{\upsilon} = 900\ cm^{-1}$ → $\dfrac{I_{AS}}{I_S} \alpha \dfrac{N_1}{N_0} = \dfrac{1}{100}$

RESONANCE RAMAN ⇒

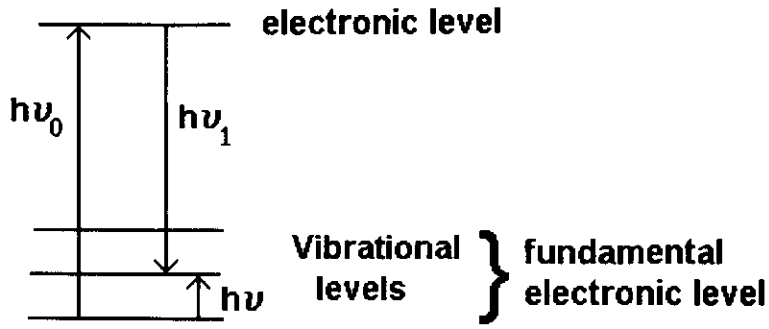

Molecule is excited with υ_o and there is an electronic transition (or, in other words, molecule absorbs light) → υ_o is a natural frequency of oscillation of the electron cloud

Excitation at these frequencies → Resonance Raman

Exciting with υ_o → increased oscillating charge displacement → increased induced dipole moment → increase scattering

Enhancement Factor - up to 10^8

Excitation of specific regions of molecule →

- visible light - cromophores (heme group, retinal)
- UV light - bases of DNA and RNA (≈ 260 nm)

  Tir, Trp, Phe (≈ 280 nm)

  peptide bond (≈ 190 nm)

PROBLEM IN RESONANCE RAMAN ⇒ Fluorescence

Fluorescence signal >> Raman signal

Fluorescence obscures Raman signal

SOLUTION - Use another laser line

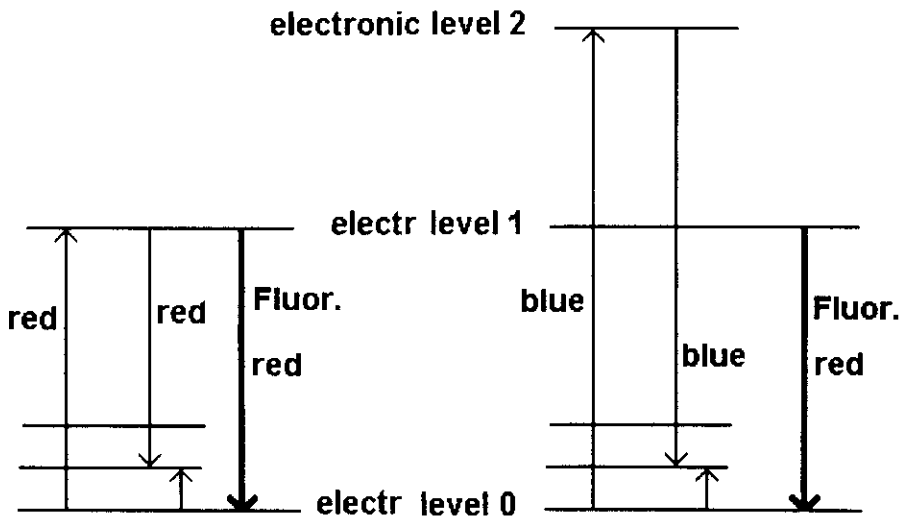

Equipment ⇒

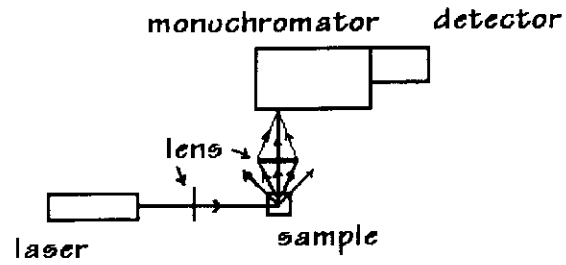

Lasers →

- CW lasers

  Ar : 514, 488, 458 nm

  He-Cd : 442 nm

- Pulsed lasers

  Nd-YAG : 1064 nm

  - Using crystal (KTP, BBO, ...):

    Overtones - 2^{nd}: 532 nm

    3^{rd}: 355 nm

    4^{th}: 266 nm

    Mix - 355 nm and 532 → 213 nm

  - Using dye lasers:

    355 nm → [Coumarin] → 420-460 nm

  - Using Raman shifter: [H_2 at high pressure]

    H-H stretching frequency: 4155 cm^{-1}

    Anti-Stokes lines

    355 nm → [H_2] → 436, 369, 320 nm

    266 nm → [H_2] → 240, 218, 200 nm

UV LASERS ! ! !

Sample Handling →

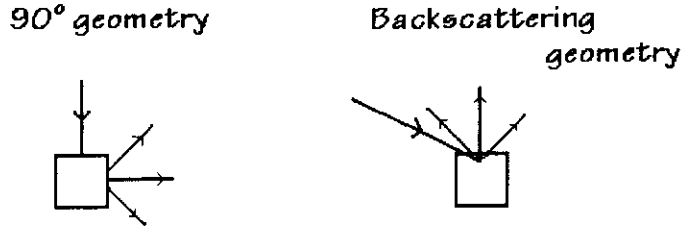

PROBLEM (mostly in Resonance Raman): laser intensity

May cause: photodegradation
heating

For solutions:

- freeze
- rotate
- flow through a capillary or as a liquid jet → needs a lot of material
- stir

For crystals, films and powders: Freeze

Monochromator → usually double or triple

$$\frac{I_{Raman}}{I_{Rayleigh}} = 10^{-6} - 10^{-9}$$

Detector →

photomultiplier
diode array
CCD (charge coupled device)

Model System for Proteins ⇒ N-methylacetamide

ATTENTION: Intensity of bands may vary for different laser lines

Position of bands doesn't change

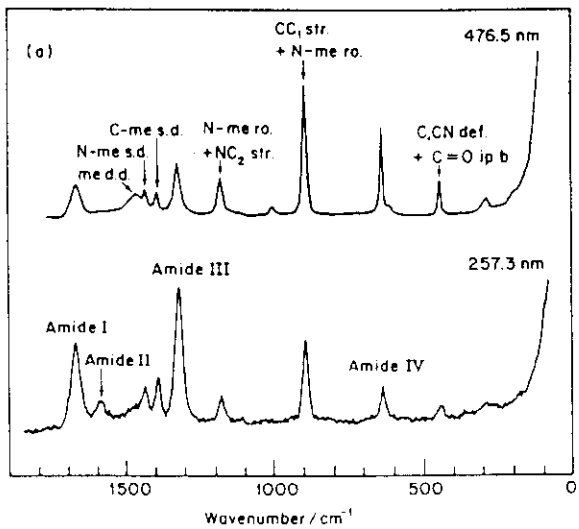

I. Harada & H. Takeuchi (1986)

Same as in IR spectroscopy → vibrational bands

However some modes may be active for IR and not for Raman,

and vice-versa (different selection rules)

IR ⇒ intense bands if vibrational motion changes electric dipole moment of the group (N-H, O-H, C=O)

RAMAN ⇒ intense bands if vibrational motion changes polarizability of the group (C=C, C-C)

▷ Proteins and Polypeptides ⇒

- Amide I and III → related to protein conformation

Drawback → low intensity of Amide I band

Mathematical methods:

Fourier deconvolution

Curve fitting

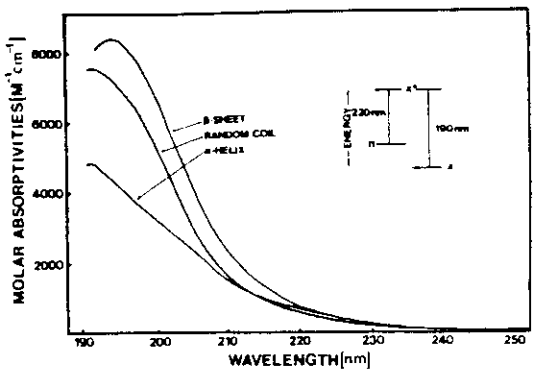

Figure 1. UV absorption spectra of aqueous solutions of poly(L-lysine) and an energy level diagram showing the electronic transitions.[37] β-sheet, pH = 11.2, 52 °C. Random coil, pH = 4.1, 25 °C. α-helix, pH = 11.0, 25 °C.

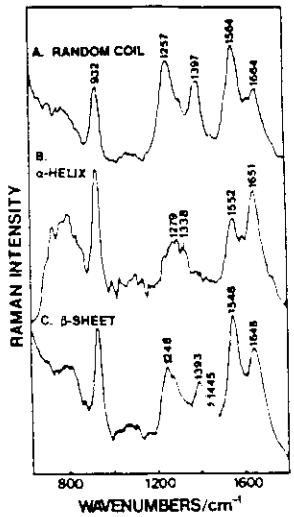

Figure 2. Raman spectra of PGA (0.11 mM) in water at 218-nm excitation, with $NaClO_4$ (0.2 M). The 932-cm^{-1} band derives from ClO_4^- stretching. (A) random coil form, pH = 10.0, 25 °C; (B) α-helix form, pH = 4.3, 25 °C; (C) β-sheet form, pH = 4.3, 95 °C.

S. Song & S.A. Asher (1989)

TABLE I

RAMAN ACTIVE BACKBONE AND SIDE CHAIN VIBRATIONS OF PROTEINS

Origin and frequency (Δcm^{-1})	Assignment	Structural information	Refs.
Backbone			
Skeletal acoustic 25–30	Mode of large portion of protein; possibly intersubunit mode or side-chain torsion	Overall structure; subunit interactions	39–41
75	Torsion mode	α Helix	41
Skeletal optical 935–945 (950 D_2O)	C–C stretch (or C^α–C–C stretch)	α Helix	33, 42–45
900	C–C stretch	These broaden and lose intensity with denaturation	33
963	—	Suggestive of β-pleated sheet	33
1002 (H_2O)	C^α–C′ or C^α–C^β stretch	—	
1012 (D_2O)	—	Conformation change marker broadens and loses intensity with denaturation	44
1100–1110	C–N stretch		
Amide I	Amide C=O stretch coupled to N–H wagging	Strong band; hydrogen bonding lowers amide I frequencies (see text)	31, 33, 46
1655 ± 5	—	α Helix (H_2O)	31, 33
1632 (D_2O)	—	α Helix (D_2O)	33
1670 ± 3	—	Antiparallel β-pleated sheet	31, 33, 46
1661 ± 3 (D_2O)	—	α Helix (D_2O)	33, 45
1665 ± 3	—	Disordered structure (solvated)	33, 45
1658 ± 2 (D_2O)	—	—	33, 42
Amide III	N–H in plane bend, C–N stretch	Strong hydrogen bonding raises amide III frequencies	33, 44
>1275	Amide III weak	α Helix, no structure below 1275 cm^{-1}	33, 44
1235 ± 5 (sharp)	Amide III strong	Antiparallel β-pleated sheet	33, 44
983 ± 3 (D_2O)	Charged coil?	Disordered structure	33, 43
1245 ± 4 broad	Charged coil?	Disordered structure	33, 43
Amino acid chains			
Tyrosine doublet			

W.L. Peticolas (1995)

TABLE I (*continued*)

Origin and frequency (Δcm^{-1})	Assignment	Structural information	Refs.
850/830	Fermi resonance between ring fundamental and overtone	State of tyrosine —OH I_{850}/I_{830} = 9:10 to 10:3, H bond from acidic proton donor; 10:9 to 3:10, strong —OH bond to negative proton acceptor	47
Tryptophan 880/1361	Indole ring	Ring environment; sharp intense line for buried residue; intensity diminished on exposure or environmental change	48, 49
Phenylalanine 1006	Ring breathing	Conformation-insensitive frequency/intensity reference	4
624	Ring breathing	Ratio with tyrosine 664 cm^{-1} to estimate Phe/Tyr	4
Histidine 1409 (D_2O)	*N*-Deuteroimidazole	Possible probe of ionization state, metalloprotein structure, proton transfer	4
S—S— 510	S–S stretch	Gauche–gauche–gauche; broadening and/or shifts may indicate conformational heterogeneity among disulfides	50–52
525	S–S stretch	Gauche–gauche–trans	50–52
540	S–S stretch	Trans–gauche–trans	50–52
C—S 630–670	C–S stretch	Gauche	50–52
700–745	C–S stretch	Trans	50–52
S—H 2560–2580	S–H stretch		
	Environment, deuteration rate	46, 51, 53, 54	
Carboxylic acids 1415	 stretch	State of ionization	4
1730	 , C=O stretch	Metal complexation	4
	 , C=O stretch		

H.Susi & M. Byler (1988)

Fourier deconvolution of Amide I Raman band of proteins

Laser line - 514.5 nm, 250 mW

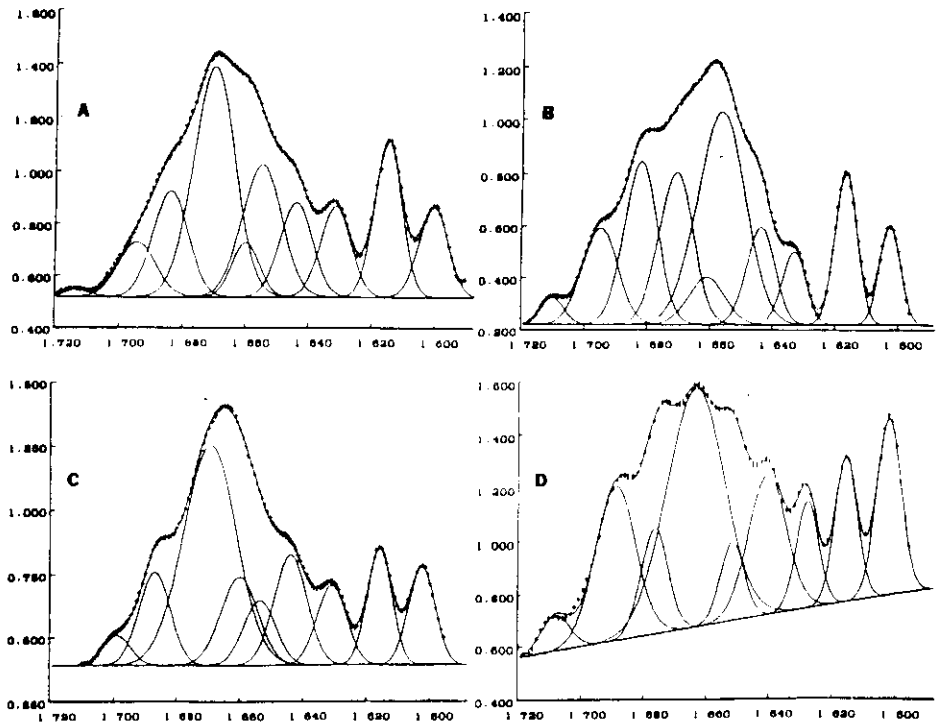

FIG. 5. Deconvolved and curve-fitted amide I Raman bands: (A) ribonuclease A; (B) lysozyme; (C) β-lactoglobulin; (D) β-casein.

Characteristic Amide I Frequencies (cm^{-1})

β-strands		Helix	Undefined	Turns		
1632	1672	1656	1661	1683	1689	1696

Estimation of Protein Conformation

	% HELIX			% β-STRAND			% OTHER		
PROTEIN	Ram	IR	x ray	Ram	IR	x ray	Ram	IR	x ray
Ribonucl.	21	21	22	50	50	46	29	29	32
Lysozyme	43	41	45	25	21	19	32	38	36
β-lactogl.	10	10	7	54	50	51	36	40	42
β-casein	7	7	-	19	21	-	74	72	-

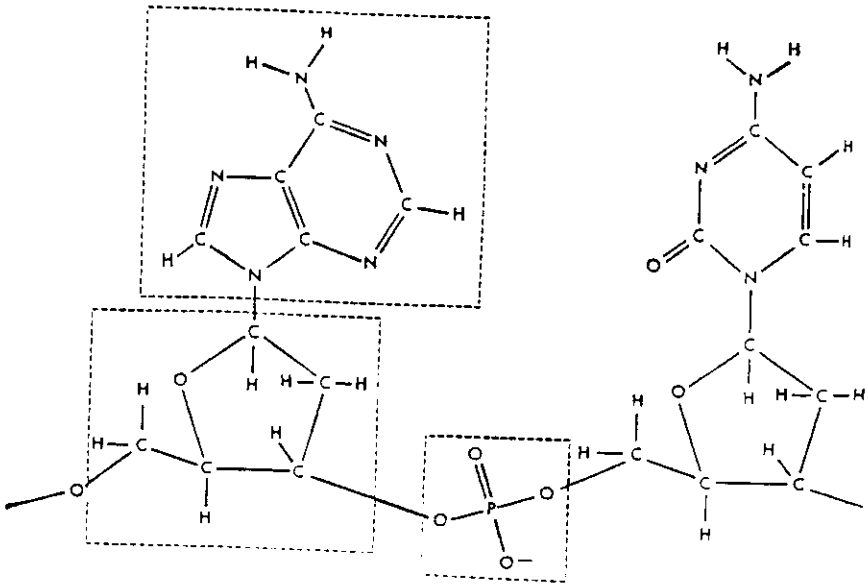

URIDINE

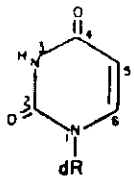

THYMIDINE

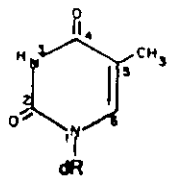

CYTIDINE

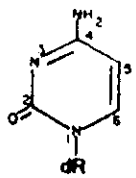

GUANOSINE

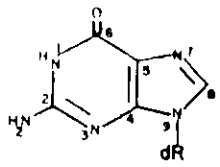

ADENOSINE

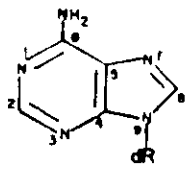

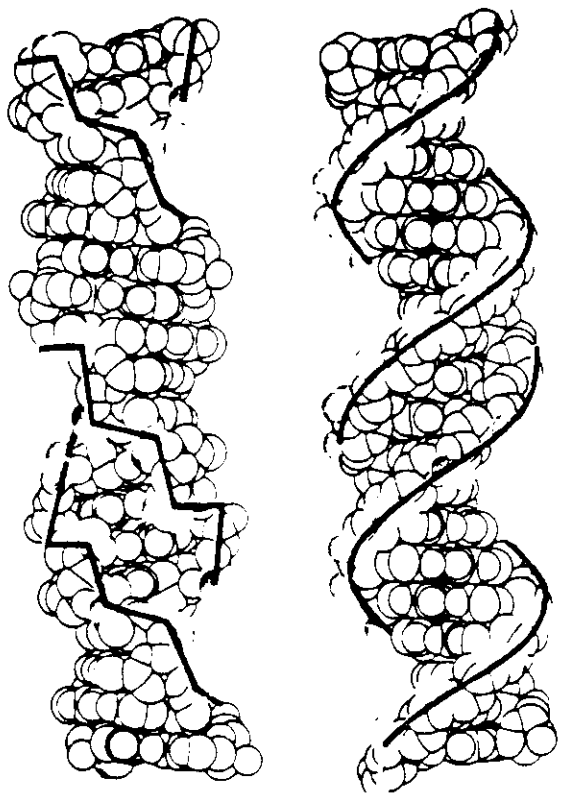

DNA de forma Z

DNA de forma B

Solução 4 M NaCl

Solução 0,5 M NaCl

$(G\text{-}C)_{30}$

poli(d(G-C)) • poli(d(G-C))

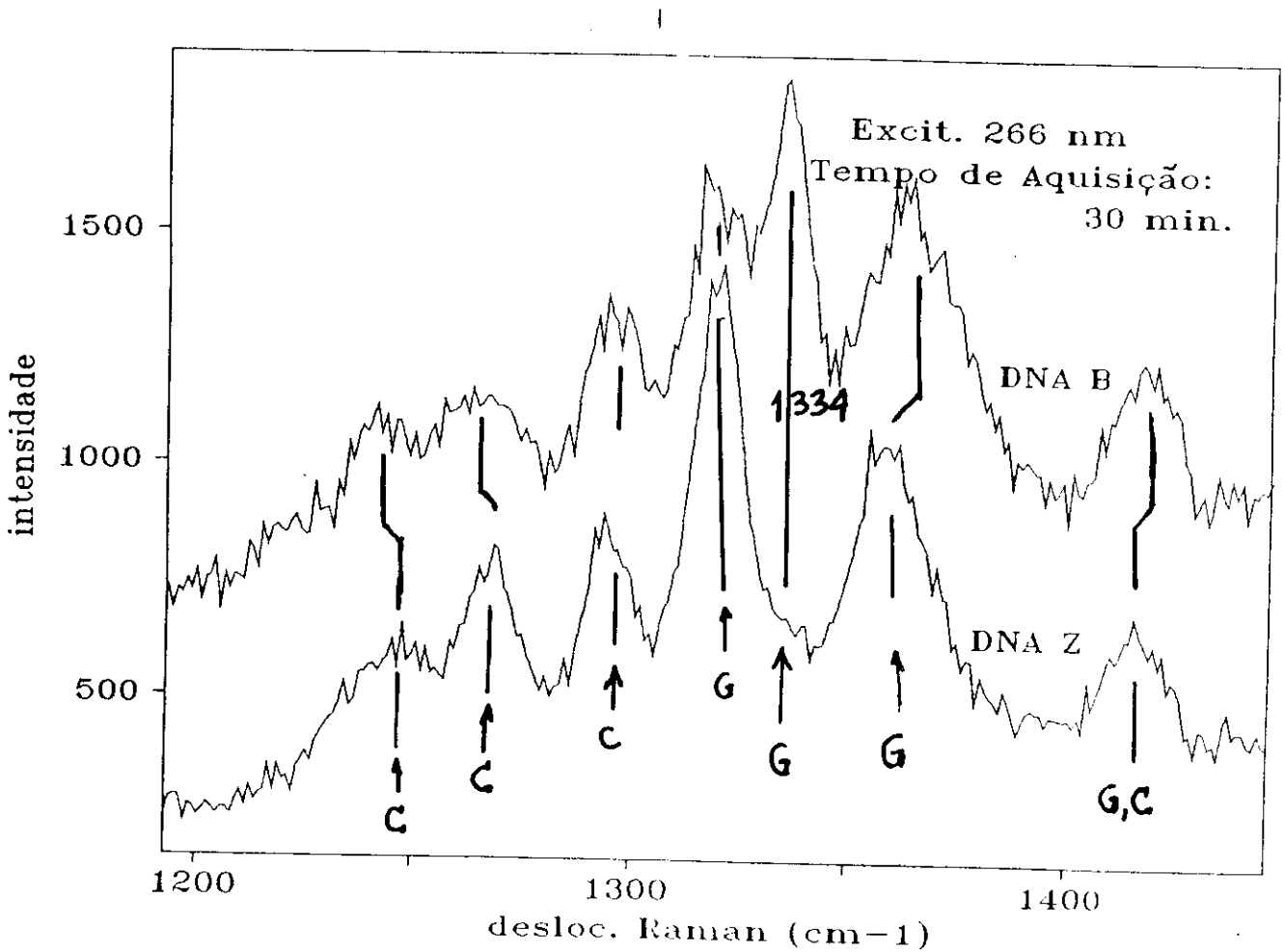
Excit. 266 nm
Tempo de Aquisição:
30 min.
DNA B
DNA Z
1334
C
C
C
G
G
G
G,C
intensidade
1500
1000
500
1200
1300
1400
desloc. Raman (cm−1)

Raman Spectroscopy of human lens lipid membranes

D. Borchman et al.

Current Eye Research 511 (1995)

Studies on structural features in the membranes of epithelium, cortex and nucleus of human lens

Importance: changes in lipid composition in human lens with age and cataract

Excitation: 1.064 μm

CH_2 stretching band and lipid order ⇒

$\frac{I_{2880}}{I_{2850}}$: order parameter

higher ratio → more ordered lipids

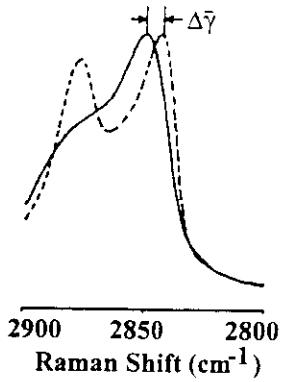

Figure 1. FT-Raman spectra of CH_2 stretching region for a typical lens lipid completely disordered in chloroform (solid) and for anhydrous dipalmitoylphospatidylcholine (dashed) in its completely ordered state.

For the lens lipids ⇒

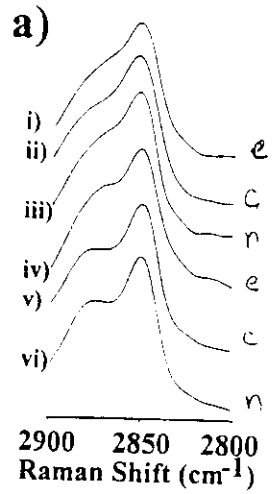

CH_2 stretching:
epithelium lipids are more disordered than cortex and nucleus lipids

Figure 2. FTRaman spectra a) CH stretching region and b) C–C acoustic stretching region of human lens lipids completely disordered in chloroform: i) epithelium; ii) cortex; iii) nucleus, and in 5 mM HEPES buffer (pH 7.4, 100 mM KCl): iv) epithelium; v) cortex; vi) nucleus.

C-C stretching:

Bands at 1063 and 1128 cm^{-1} → C-C in all trans conformation

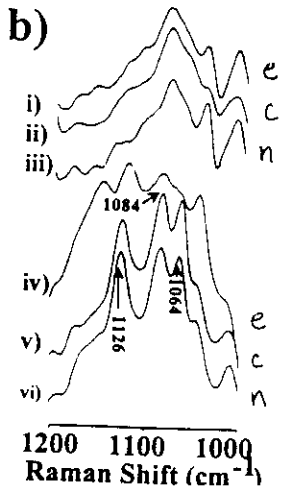

Bands for epithelium lipids are smaller → less all trans conformation → more disorder

Disorder in human lens lipids from the epithelium due to high phosphatidylcholine to sphingomyelin ratio

All calcium pumps, critical to clarity of human lens, are located in the epithelium

A disordered matrix may be essential for calcium pump activity

In cataractous lenses → lower calcium pump activity

Raman Studies on the Interaction of Trehalose with Hen Egg White Lysozyme

P.S. Belton & A.M. Gil
Biopolymers 34, 957 (1994)

Trehalose - a disaccharide found in resurrection plants → found in deserts in South America subjected to high temperatures (up to 60°C) and extremely dry conditions
- is believed to be responsible for protection of plants against effects of heat and dehydration

Study: dried mixture of Trehalose and lysozyme compared to dried lysozyme

Raman spectra ⇒ Excitation 1064 nm

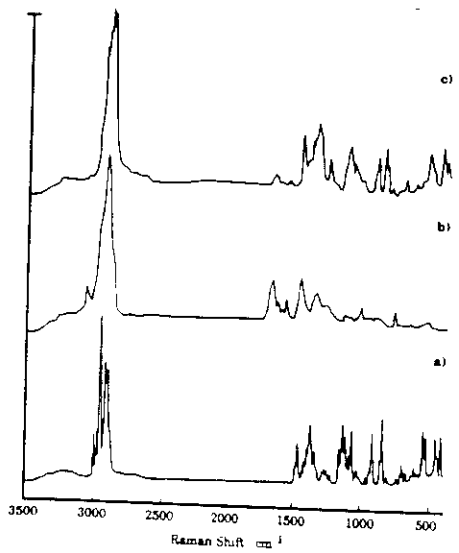

Figure 1. FT Raman spectra of (a) trehalose dihydrate, (b) dry lysozyme powder, and (c) dry lysozyme/trehalose 1 : 10 powder.

Trehalose → no band in 1700-1500 cm^{-1} region

Amide I and II regions ⇒

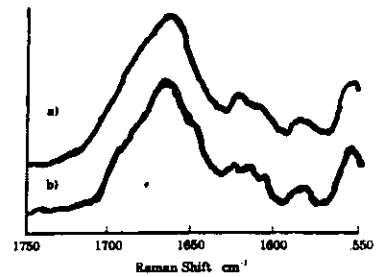

Figure 2. Expansions of the 1750–1550 cm^{-1} regions of the FT Raman spectra of (a) dry lysozyme powder and (b) dry lysozyme/trehalose 1 : 10 powder.

Narrower bands in mixture → conformational changes in lysozyme

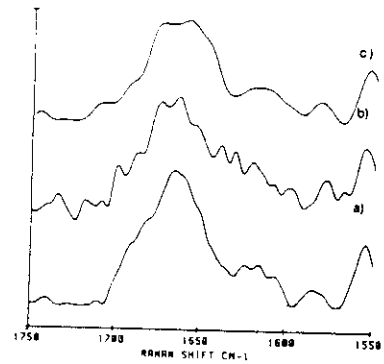

Figure 3. FT Raman spectra of hydrated samples of (a) lysozyme, 20% water and (b) lysozyme/trehalose 1 : 10, 18% water at 4 cm^{-1}, and at (c) 8 cm^{-1} resolution.

Water causes similar conformational changes

Hypothesis:

In solution sugar is excluded from proximity of protein by water

As system dries water concentrates at protein/sugar interface and is trapped there by glass formation

Raman Study of Butyrylcholinesterase

D. Aslanian, P. Gróf, F. Renault & P. Masson

Biochim. Biophys. Acta 1249, 37 (1995)

Human butylrylcholinesterase (BuChE):

- Native state
- Conjugated with organophosphates

Studies of:

- secondary structure - Amide I band
- vibrations of aromatic groups

BuChE- 574 amino acids (39 phe, 20 tyr, 18 trp)

- present in human plasma
- main target of organophosphorous inseticides, pesticides and nerve agents

Used: paroxan

DFP (diisopropylphosphofluoridate) ↘

soman ——————→

→ enzyme cannot be reactivated - "aged" BuChE

Samples: 15 mg/ml in Tris buffer pH 7.5, temperature 10°C

Excitation: 514.5 nm, 130 mW

Raman Spectra

- Trp vibration ≈ 1360 cm^{-1}
  - sharp peak when trp buried in hydrophobic environment
  - low intensity when trp is in hydrophilic environment (as in native BuChE)

DFP-BuChE and Soman-BuChE → trp in a more hydrophobic environment

- Secondary structure
  - Subtraction of aromatic amino acid contributions in Amide I region

"aged" BuChE → decrease in α-helix
increase in β-sheets

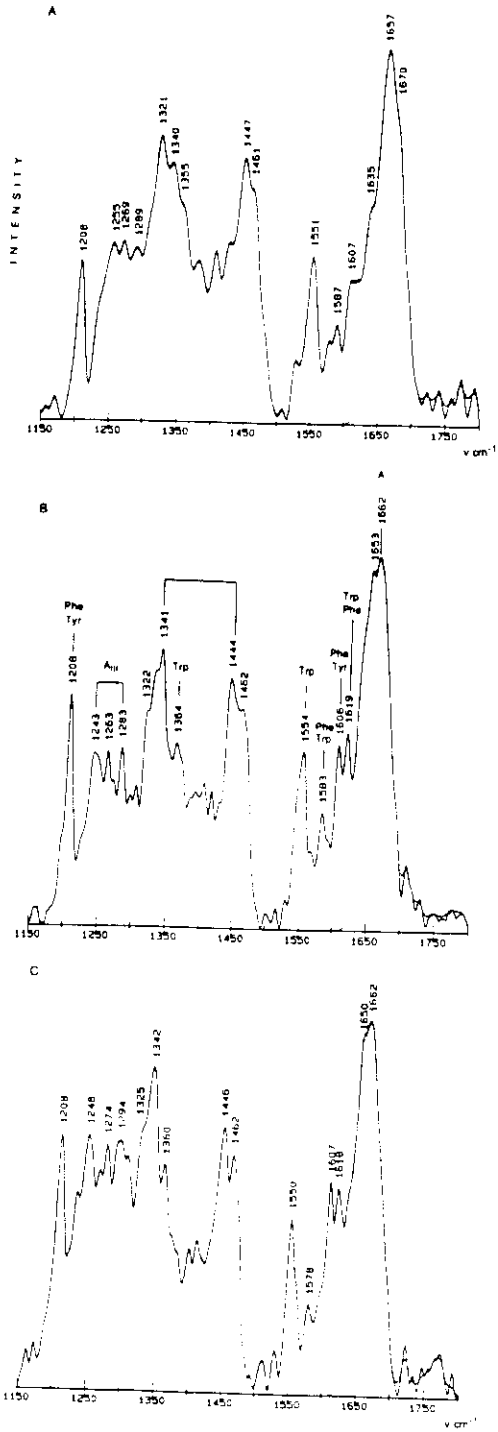

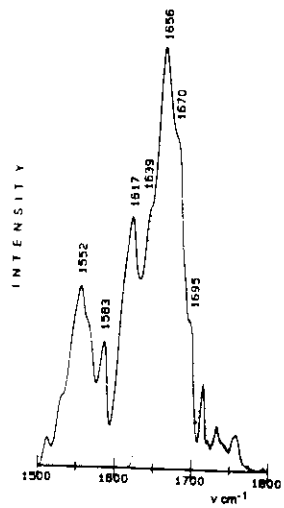

Fig. 2. Amide I region of paraoxon-phosphorylated BuChE before (—) and after (· · ·) subtraction of aromatic amino-acid vibrations.

Table 1
Quantitative estimation of secondary structure elements for native and OP-inhibited BuChE

Enzyme	Structure (%)			
	α_t (α_o α_d)	β_t (β_{ap} β_p)	T	U
Native	47 (28 19)	26 (25 1)	16	12
Paraoxon-inhibited	46 (34 12)	29 (28 1)	14	10
DFP-'aged'	39 (31 8)	31 (28 3)	17	13
Soman-'aged'	36 (32 4)	34 (30 4)	20	10

α_t, total α-helix; α_o, ordered α-helix; α_d, disordered α-helix; β_t, total β-sheets; β_{ap}, antiparallel β-sheets; β_p, parallel β-sheets; T, turns; U, undefined.

Fig. 1. (A) Raman spectrum of native BuChE in 10 mM Tris-HCl (pH 7.5). Recording conditions are given in the text. (B) Raman spectrum of 'aged' DFP-BuChE conjugate. (C) Raman spectrum of 'aged' soman-BuChE conjugate. (· · ·) amide I regions after subtraction of aromatic amino-acid vibrations.

References

General:

1) I. Harada and H. Takeuchi, Raman and Ultraviolet Raman Spectra of Proteins and Related Compounds *in Spectroscopy of Biological Systems, ed.* R.J.H. Clark and R.E. Hester (1986) John Wiley & Sons, pp. 113

2) S.A. Asher, UV Resonance Raman Studies of Molecular Structure and Dynamics: Applications in Physical and Biophysical Chemistry, Ann. Rev. Phys. Chem. 39, 537 (1988)

3) T.G. Spiro, Probing Biological Molecules with Lasers, Chemistry in Britain, June 1989, pp. 602

4) S.A. Asher, UV Resonance Raman Spectroscopy for Analytical, Physical and Biophysical Chemistry, Anal. Chem. 65, 59A (1993)

5) W.L. Peticolas, Raman Spectroscopy of DNA and Proteins, Methods Enzymology 246, 389 (1995)

6) T.G. Spiro and R.S. Czernuszewicz, Resonance Raman Spectroscopy of Metalloproteins, Methods Enzymology 246, 416 (1995)

7) P.J. Hendra, H.M.M. Wilson, P.J. Wallen, I.J. Wesley, P.A. Bentley, M. Arruebarrena-Baez, J.A. Haigh, P.A. Evans, C.D. Dyer, R. Lehnert and M.V. Pellow-Jarman, Routine Analytical

Fourier Transform Raman Spectroscopy. Part 2: Un Updated Review, Analyst 120, 985 (1995)

Applications

• Structure Estimation

8) G.J. Thomas Jr. and D.A. Agard, Quantitative Analysis of Nucleic Acids, Proteins and Viruses by Raman Band Deconvolution, Biophys. J. 46, 7763 (1984)

9) H. Susi and D.M. Byler, Fourier Deconvolution of the Amide I Raman Band of Proteins as Related to Conformation, Appl. Spectr. 42, 819 (1988)

10) S. Song and S.A. Asher, UV Resonance Raman Studies of Peptide Conformation in Poly(L-lysine), Poly(L-glutamic acid), and Model Complexes: the Basis for Protein Secondary Structure Determination, J. Am. Chem. Soc. 111, 4295 (1989)

11) T.M. Przybycien and J.E. Bailey, Secondary Structure Perturbations in Salt-induced Protein Precipitates, Biochim. Biophys. Acta 1076, 103 (1991)

•Other Applications

12) P.R. Carey and P.J. Tonge, Unlocking the Secrets of Enzyme Power Using Raman Spectroscopy, Acc. Chem. Res. 28, 8 (1995)

13) V. Jayaraman, K.R. Rodgers, I. Mukerji and T.G. Spiro, Hemoglobin Allostery. Resonance Raman Spectroscopy of Kinetic Intermediates, Science 269, 1843 (1995)

Spectroscopy 4

Applications of Photoacoustic, Raman and Infrared Spectroscopies in Biology

Rosemary Sanches
Dept. Física e Informática
Instituto de Física de São Carlos
Universidade de São Paulo
Brazil

In Vivo Studies in Plant Photosynthesis

H. Vargas et. al.

Meas. Sci. Technol. 3, 931 (1992)

$$nCO_2 + nH_2O \Rightarrow (CH_2O)_n + nO_2$$
$$\downarrow$$
carbohydrate

Photoacoustic Signal:

(1) Photothermal contribution (non-radiative de-excitation process)

(2) Photobaric contribution (oxygen evolution)

(3) Photochemical loss (energy storage) (2)>(3)

+ non-modulated white light → saturation of the photosynthetic apparatus

∴ PAS = (1)

Low modulation frequency → PAS = (1)+(2)-(3)

+ white light → PAS = (1) ⇒ Negative Effect

High modulation frequency → PAS = (1)-(3)

slow O_2 diffusion

+ white light → PAS = (1) ⇒ Positive Effect

Corn Leaf : *In situ* measurements

Soybean Leaf : *In situ* and detached measurements

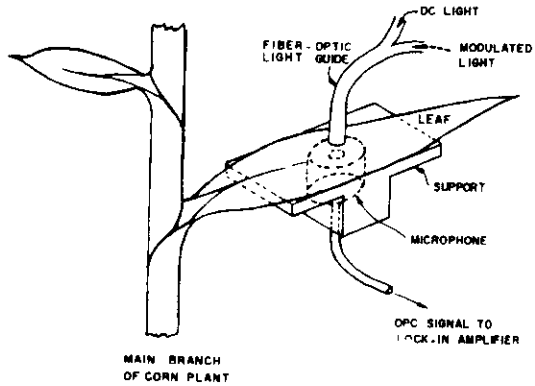

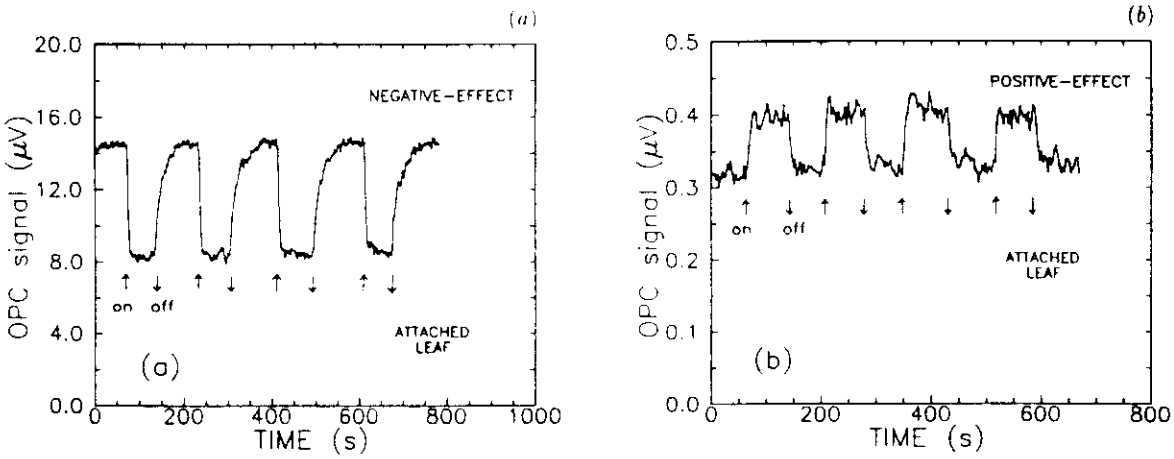

Figure 3. Effect of background light (220 W m^{-2}) application on the OPC signal at two frequencies. At 19 Hz the negative effect in corn leaf (*a*) and at 500 Hz the positive effect in soybean leaf (*b*). We used modulated light 680 nm, 9.7 W m^{-2}. These effects are related to the measures of oxygen evolution (*a*) and storage energy (*b*).

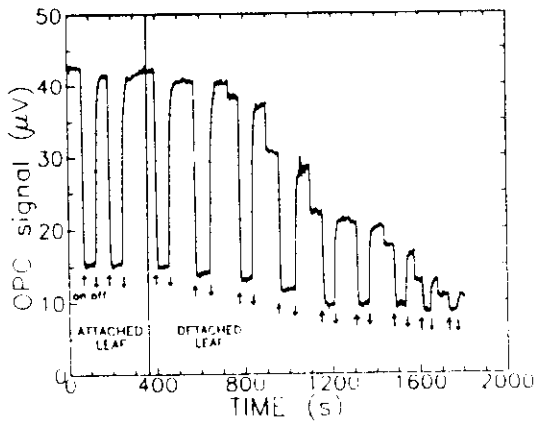

Figure 4. Effect of leaf dehydration on photochemical activities in soybean leaf. The negative effect is constant until the leaf is detached from the plant, after which it decreases. We used modulated light 680 nm, 9.7 W m^{-2} and white light 220 W m^{-2}. Modulation frequency, 19 Hz.

Electron Transfer in a Model System

M.L. Cornélio & R. Sanches
Eur. Biophys. J. 23, 439 (1995)

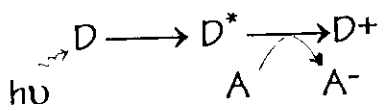

Interest: Photosynthesis
Molecular Electronics

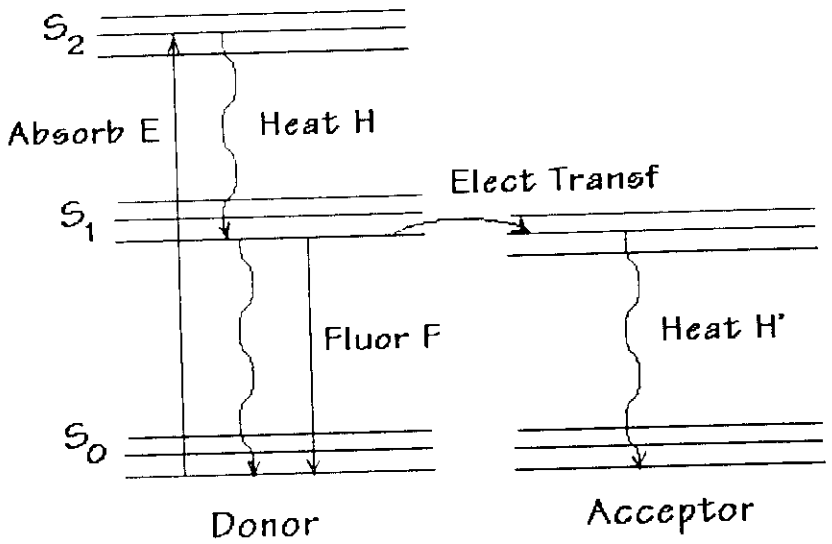

Without A ⇒

$E = H_0 + F_0$

With A ⇒

$E = H + F + H'$

$\therefore$

$F = E - (H+H')$

More Electron Transfer ⇒ Less Fluoresc. (Quenching)
Electron Transfer depends on [A] ⟶ MODELS

More Electron Transfer ⇒ More H' ⇒ Enhanced PAS
Fluoresc. ⇓ and PAS ⇑ → Complementary Processes
Use same MODELS

$H_t = H + H' = E - F$

SAMPLES:

Films { Donor: OEP (porphyrin) [OEP] fixed
Acceptor: DQ (quinone) [DQ] varied
Matrix: PMMA

Random distribution of D and A molecules

PERRIN MODEL :

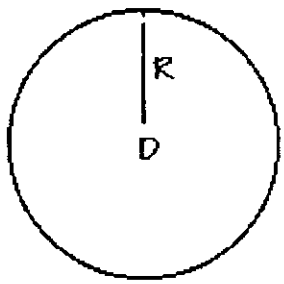

sphere

R: critical radius for electron transfer

If A inside sphere → electron transfered

If A outside sphere → no electron transfered

Fluorescence Quenching:

$$F = F_0 e^{-V[A]}$$

Expected for PAS:

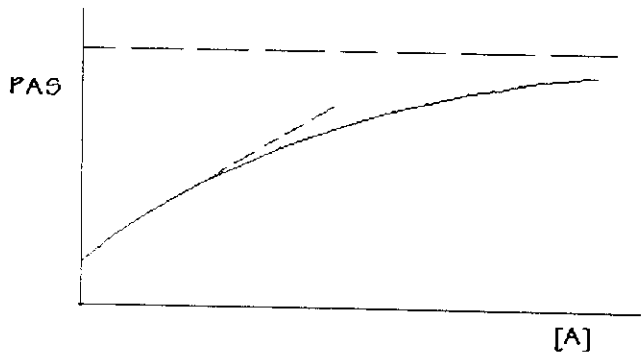

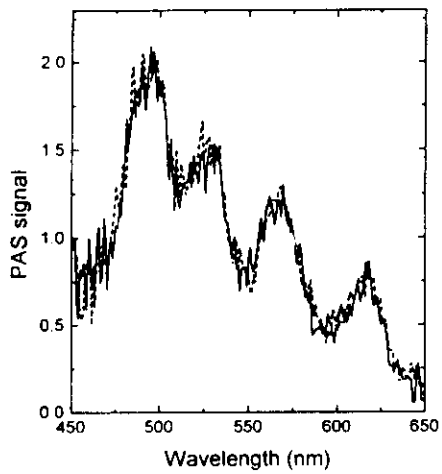
PAS signal
Wavelength (nm)

(a)

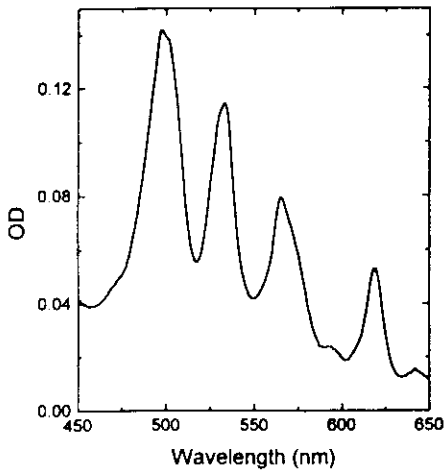
OD
Wavelength (nm)

(b)

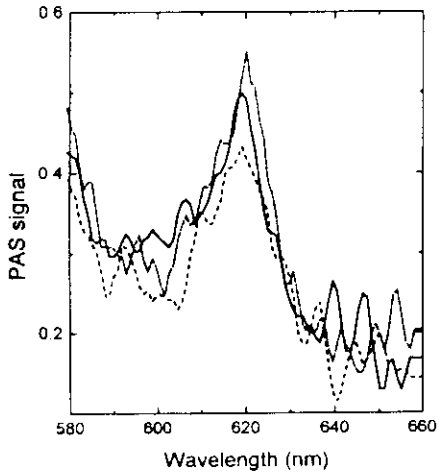
PAS signal
Wavelength (nm)

(a)

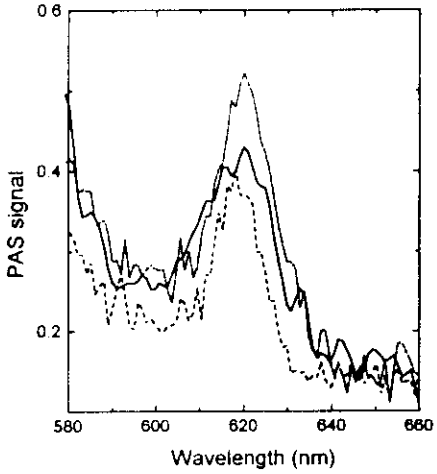
PAS signal
Wavelength (nm)

(b)

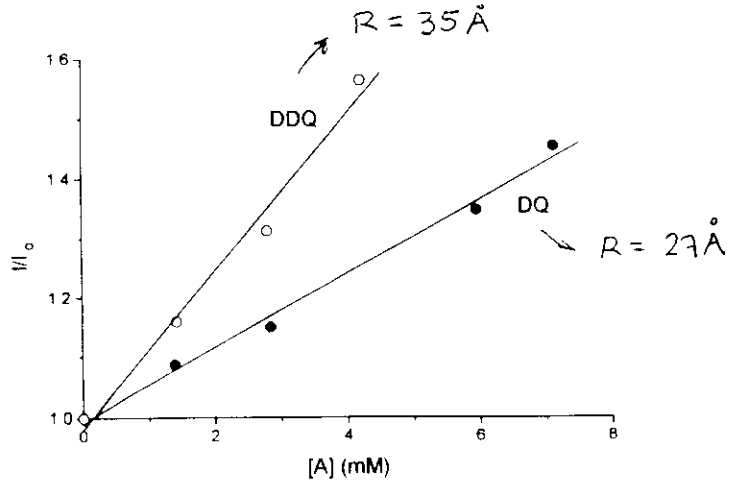
R = 35 Å
DDQ
DQ
R = 27 Å
I/I0
[A] (mM)

Study of Protein Secondary Structure by FT-IR/Photoacoustic Spectroscopy

S. Luo, C-Y. F. Huang, J.F. McClelland & D.J. Graves

Analytical Biochemistry 216, 67 (1994)

Studied: concanavalin A
hemoglobin
lysozyme
trypsin

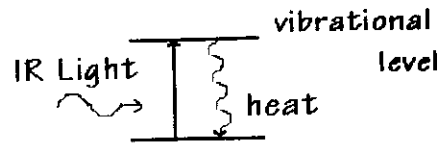

Samples: dissolved in 1% NaCl (pH 6.5)
≈ 2 μl of protein solution (conc. 0.5-3 μg/μl) spread on a Teflon disk

Analysis of Amide I Band ⇒
- Water bands subtracted
- Secondary derivative
- Curve fitting (Gaussian)

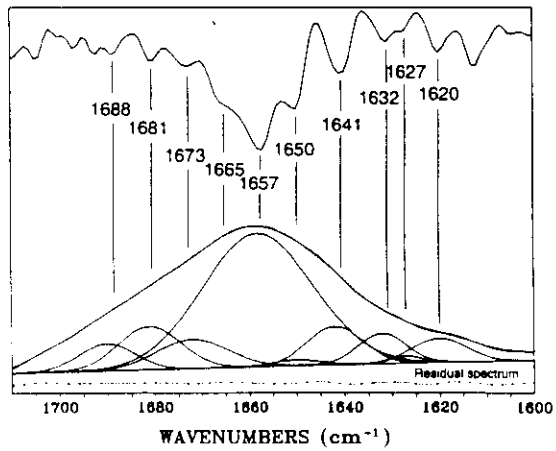

FIG. 2. Infrared spectrum and calculated curve fit spectrum of lysozyme (middle), its secondary derivative spectrum (top), and curve-fitting result (bottom).

TABLE 1

Comparison of Peak Position of Lysozyme with Different Methods

Methods	Peak positions (cm^{-1})										
FT-IR/PAS	1688	1681	1673	1665	1657	1650	1641		1632	1627	1620
FT-IR(3)	1688	1680	1672	1666	1657	1650	1642	1639	1632	1627	
Raman(24)	1695	1682	1671	1662	1658		1644		1633		

Secondary Structure of Proteins ⇒

TABLE 2

Comparison of Secondary Structure of Four Standard Proteins with Different Methods

Protein	Methods	Secondary structure (%)				Ref.
		α-Helix	β-Sheet	Turn	Random	
Concanavalin A	FT-IR/PAS	16	58	20	6	
	FT-IR	8	58	26	8	(3)
	X-ray	3	60	22	15	(31)
	CD	3–25	41–49	15–27	3–25	(34–36)
Hemoglobin	FT-IR/PAS	72	10	18		
	FT-IR	78	12	10		(3)
	X-ray	87	0	7	6	(31)
	CD	68–75	1–4	15–20	9–16	(33, 37)
Trypsin	FT-IR/PAS	11	49	35	5	
	FT-IR	9	44	38	9	(3)
	X-ray	9	56	24	11	(31)
Lysozyme	FT-IR/PAS	56	27	16	1	
	FT-IR	40	19	27	14	(3)
	X-ray	45	19	23	13	(31)
	CD	29–45	11–39	8–26	8–60	(32–38)

CAUTION:

Photoacoustic Saturation ⇒

No linear correlation of concentration and peak height

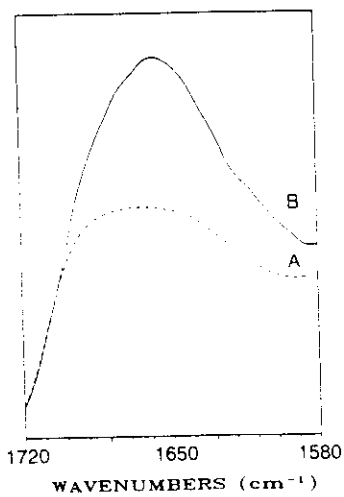

FIG. 5. Spectra of lysozyme in powder form (A) and in the layer form (B).

FT-IR Studies on the Secondary Structure of Concanavalin in Halogenated Alcohols

M. Jackson & H.H. Mantsch
Biochim. Biophys. Acta 1118, 139 (1992)

* Chloroethanol and trifuoroethanol are good solvents for proteins and are used as membrane mimetic agent

However:

- Dielectric constant: $\varepsilon_{membrane} \approx 1$
  $\varepsilon_{ClEt} \approx 25.8$
  $\varepsilon_{3FEt} \approx 26.6$
- Halogenated alcohols contain potent H bond donor → disrupt secondary structure of protein. Evidences that they induce helical conformation in polypeptide chains

QUESTION: Are halogenated alcohols helicogenic?

Samples:

Conc.: 10mg/ml

ℓ = 6 μm for samples in alcohols

ℓ = 50 μm for samples in D_2O

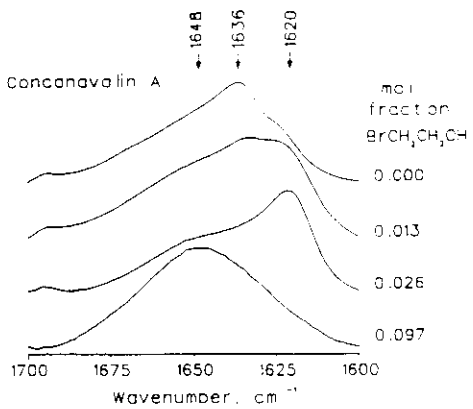

Fig. 1. Infrared absorbance spectrum in the amide I region of concanavalin A in ^2H_2O and ^2H_2O /bromoethanol mixtures.

In D_2O →

1636 cm^{-1} → predominance of β-sheet structure

1650 cm^{-1} → α-helix

1625 cm^{-1} → interaction of β-strand with solvent

Low concentration of BrEt →

increase ≈ 1620 cm^{-1} → characteristic od protein denaturation → disruption of H bonds within some secondary structure and formation of stronger intermolecular H bonds → aggregation

Increasing concentration of BrEt → concanavalin A is insoluble → Alcohol and D_2O molecules are H bonded to each other

Higher concentration of BrEt → Amide I band maximum changes from 1648 to 1654 cm^{-1} (last value in pure alcohol) → due to decrease in deuteration of protein amide groups

Which is this new structure?

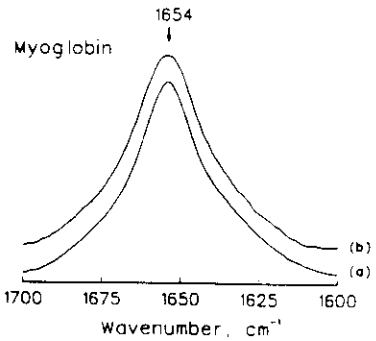

Fig. 2. Infrared absorbance spectra in the amide I region of myoglobin in pure chloroethanol (a) and in H_2O (b).

Similar spectra → Helical structure present in Mb in ClEt

Similar to concanavalin A spectra → new structure is α-helical configuration

Similar results with other halogenated alcohols ⇒

Helicogenicity:

2ClEt > BrEt > 3FEt > ClEt > FEt

Why helicogenicity of halogenated alcohols?

- Competition of alcohol OH group to H bond to amide C=O and N-H groups

But concanavalin a in Et → minor changes in spectrum

- Effect of alcohol upon amino acid side chains

But effect is observed in wide variety of proteins and homopolypeptides (polyala, polylys, ...)

- Effect due to lowering of dielectric constant of alcohol/water mixture, reducing tendency of non-polar residues to be in protein interior

But ClEt and Et have similar ε

Hypothesis

Combination of two factors:

- high dipole moment (D)
- relatively low dielectric constant (ε)

Et	ClEt
D = 1.71	D = 1.90
ε = 25	ε = 25.8

D has to be strong enough to disrupt protein intramolecular H bonds

ε has to be low to promote unfolding of protein and refolding in α-helical configuration

Why α-helix?

This must be most energetically stable conformation in environments with low ε

In fact → most membrane proteins are α-helical

Site-Directed Isotope Labeling and FT-IR: Assignment of Tyr Bands in bR → M Difference Spectrum of Bacteriorhodopsin

X-M. Liu, S. Sonar, C-P. Lee, M. Coleman, U.L. RajBhandary & K.J. Rothschild

Biophys. Chem. 56, 63 (1995)

Bacteriorhodopsin - protein in membrane of Halobacterium salinarium

In dark: bR state
In light: M state

▷ Study differences in Tyr environment for the two states

METHOD: site-directed isotope labeling

- 11 Tyr in bacteriorhodopsin -
  Labeled: 147 or 185 or 57 or all

- For each sample get difference spectrum:
  (M spectrum) - (bR spectrum)

- Spectrum compared to unlabeled
  No difference → no change in Tyr environment

Samples: membrane dried in AgCl window T = 250 K

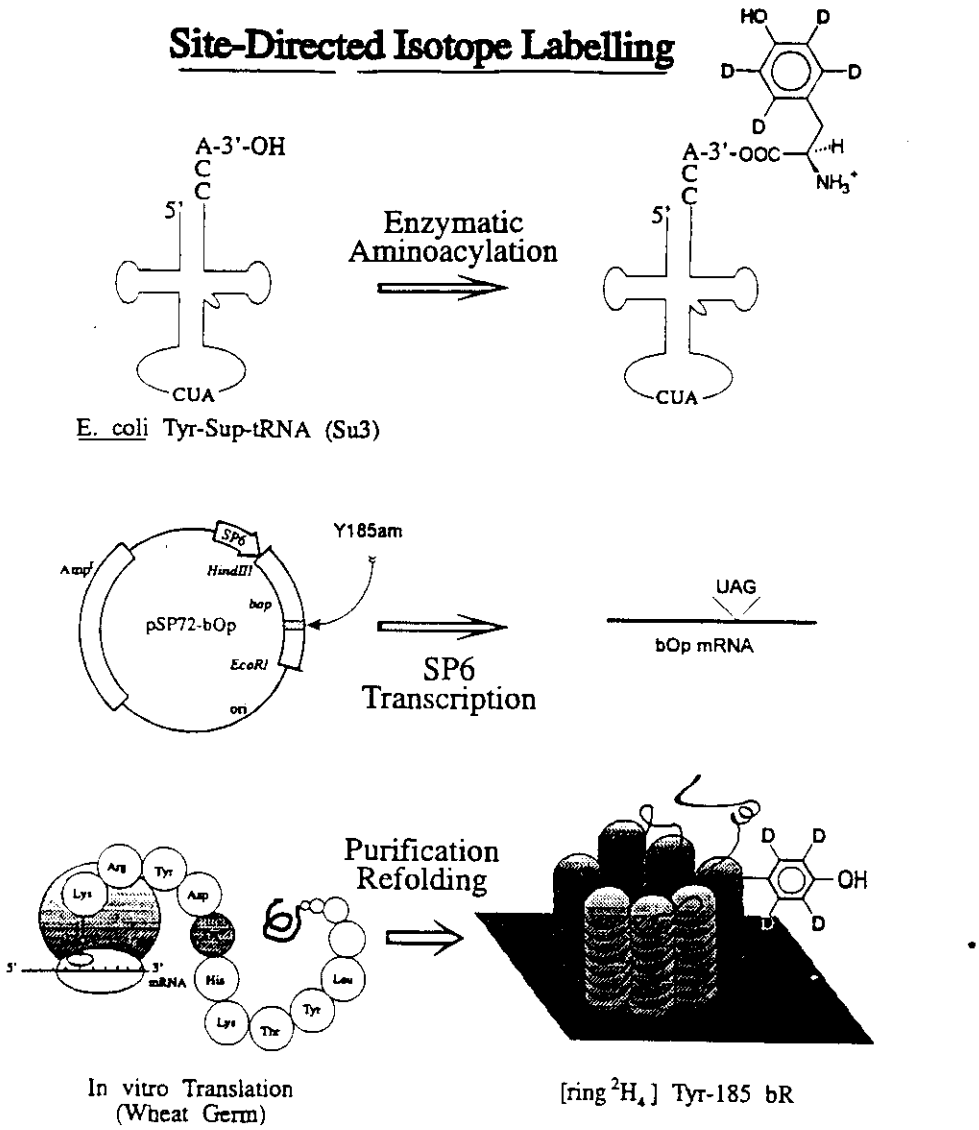

Fig. 2. Major steps in site directed isotope labeling of a protein. Top: *E. coli* tyrosine sup-tRNA is enzymatically aminoacylated with a deuterated tyrosine; middle: using recombinant DNA methods an amber codon is inserted in the gene at the position of the residue to be isotope labeled followed by mRNA synthesis using run off transcription; bottom: the mRNA is translated in a cell-free protein synthesis system in the presence of the aminoacylated suppressor tRNA. The resulting SDIL analog is then purified and refolded. (Figure adapted with permission from *Nature Struct. Biol.* (August 1994 issue)).

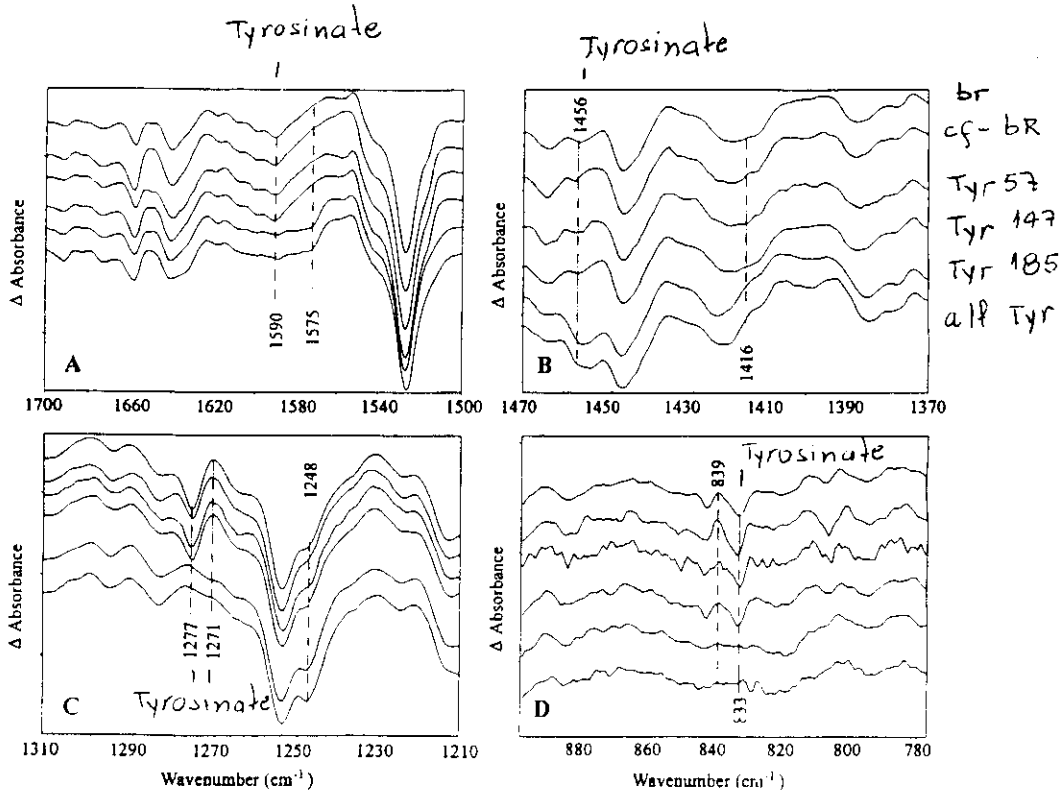

Fig. 4. Expansion in selected regions of the data shown in Fig. 3.

Spectra of Tyr57-labeled, Tyr147-labeled and unlabeled are very similar → these two residues do not undergo significant conformational changes in the bR → M transition

Spectra of Tyr185-labeled exhibits significant changes compared to unlabeled. Changes similar to the ones in the all-labeled spectrum → Tyr 185 is structurally active in the bR → M transition

FT-IR Study of Major Coat Protein of M13 and Pf1

W.F. Wolkers, P.I. Haris, A.M.A. Pistorius, D. Chapman & M.A. Hemminga

Biochemistry 34, 7825 (1995)

M13 and Pf1 → bacteriophages

Circular single-stranded DNA + several thousand copies of a major protein

During infection of bacterial cell → major coat protein in stripped off from DNA and inserted into cytoplasmic membrane of host

This study ⇒ secondary structure of major coat protein in phage and reconstituted in phospholipid bilayers

- For studies in D_2O → $\ell = 50\ \mu m$
  removal of band at 1209 cm^{-1}
- For studies of membrane →
  lipid - DOPG: dioleoyl glycero-3-phosphoglycerol
  films in AgCl window

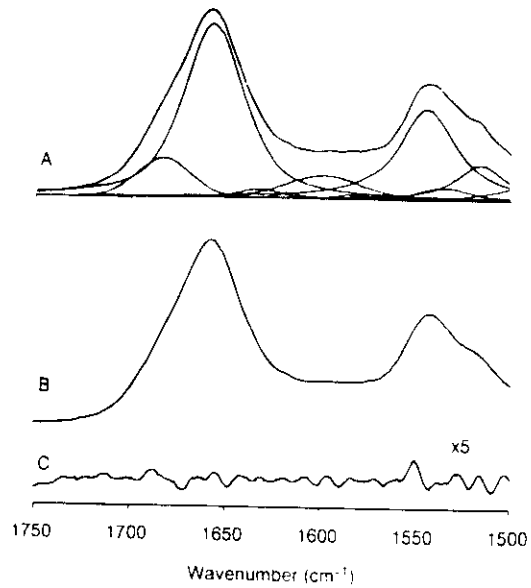

FIGURE 1: (A) FT-IR absorption spectrum of Pf1 phage particles in dehydrated film at 25 °C (top line) and the component spectra that are used to fit the spectrum according to the parameters given in Table 1. (B) Best fit of the curve fitting procedure. (C) Difference of the absorption spectrum in (A) and best fit (B) (the scale factor is 5).

Table 1: Complete Assignment of the Spectral Region between 1500 and 1800 cm⁻¹ of the FT-IR Absorbance Spectrum of Pf1 Phage in a Dehydrated Film[a]

position γ (cm^{-1})	width $\Delta\gamma$[b] (cm^{-1})	area (arb units)	relative area[a] (%)	band region	assignment
1516	15.71	3.69			Tyr
1535	16.13	1.31	11	amide II band	
1543	18.60	10.94	89	amide II band	
1574	3.43	0.05			Asp
1584	10.62	0.32			Asp
1598	24.34	3.72			Lys $\delta(NH_3^+)$
1617	7.18	0.26			Tyr
1633	13.19	0.75	3	amide I band	
1657	19.30	21.51	81	amide I band	
1683	16.83	4.32	16	amide I band	

[a] The error in the position γ and linewidth $\Delta\gamma$ is ±1 cm^{-1}; the error in the relative area is ±1% for area > 20% and ±2% for area < 20%. [b] Total width at half-height. Relative area in amide I and amide II band.

Table 3: Analysis of the Amide I Region of Pf1 Coat Protein in the Phage and Reconstituted in DOPG Bilayers at L/P 20

system	assignment	phage			DOPG		
		γ (cm^{-1})	$\Delta\gamma$ (cm^{-1})	area (%)	γ (cm^{-1})	$\Delta\gamma$ (cm^{-1})	area (%)
Pf1 (dehydrated film)	hydrogen-bonded turn	1633	13	3	1644	14	12
	α-helix and coil	1657	19	81	1658	10	58
Pf1 (D_2O suspension)	non-hydrogen bonded turn	1683	17	16	1673	19	30
	turn, coil, and disordered α-helix	1634	18	33	1640	17	43
	α-helix without disordered part	1653	15	60	1657	10	53
	non-hydrogen-bonded turn	1676	9	7	1675	12	4

Table 4: Analysis of the Amide I Region of M13 Coat Protein in the Phage and Reconstituted in DOPG Bilayers at L/P 20

system	assignment	phage			DOPG		
		γ (cm^{-1})	$\Delta\gamma$ (cm^{-1})	area (%)	γ (cm^{-1})	$\Delta\gamma$ (cm^{-1})	area (%)
M13 (dehydrated film)	β-sheet/aggregated protein				1629	10	5
	hydrogen-bonded turn	1632	10	3	1643	21	21
	α-helix and coil	1656	19	79	1657	10	50
	non-hydrogen-bonded turn	1683	17	18	1672	17	21
M13 (D_2O suspension)	β-sheet/aggregated protein				1691	14	3
	turn, coil, and disordered α-helix	1637	19	31	1640	18	56
	α-helix without disordered part	1650	14	67	1656	11	42
	non-hydrogen-bonded turn	1673	12	2	1677	6	2

▷ Coat protein ⇒

From dehydrated state to D_2O:

Pf1 1657 → 1653 cm^{-1} (81%) (60%) M13 1656 → 1650 cm^{-1} (79%) (67%)

- shift in frequency → due to D bonding of α-helix with solvent
- decrease in content → H-D exchange

Amide I band of random coil structure moves to ≈ 1640 cm^{-1}

Part of helical region may be accessible to H-D exchange

Therefore, lower limit for α-helical content ⇒

60% for Pf1 and 67% for M13

▷ Reconstituted Membrane ⇒

From dehydrated state to D_2O:

Pf1 1658 → 1657 cm^{-1} (58%) (53%) M13 1657 → 1656 cm^{-1} (50%) (42%)

- no shift in frequency → α-helix is not accessible to solvent
- decrease in content → H-D exchange

Lower limit for α-helical content ⇒

60% for Pf1 and 67% for M13

CONCLUSION: α-helical content decrease when protein is in lipid environment

Resonance Raman Studies of Myoglobin from *Nassa mutabilis* (NM) - a gastropod mollusc

G. Smulevich, A.R. Mantini, M. Paoli, M. Colleta & G. Geraci

Biochemistry 34, 7507 (1995)

- Structural studies of deoxy-Mb
  MbO_2
  met-Mb

- Comparison to horse heart myoglobin

Mb - present in muscle cells

- usually monomeric, but in NM → homo-dimeric with cooperative O_2 binding

Excitation lines: 406.7, 413.2, 530.9, 457.9 nm

Heme group absorption ⇒

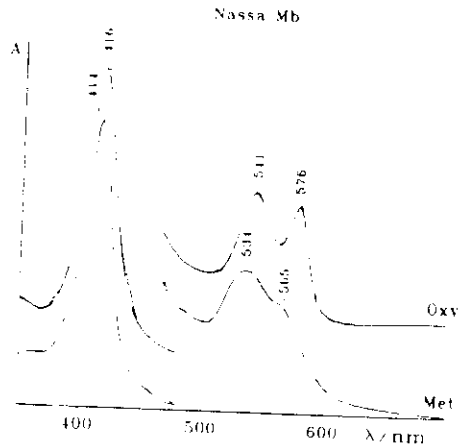

FIGURE 8: Electronic absorption spectra of oxy- and met-Mb from *Nassa mutabilis*.

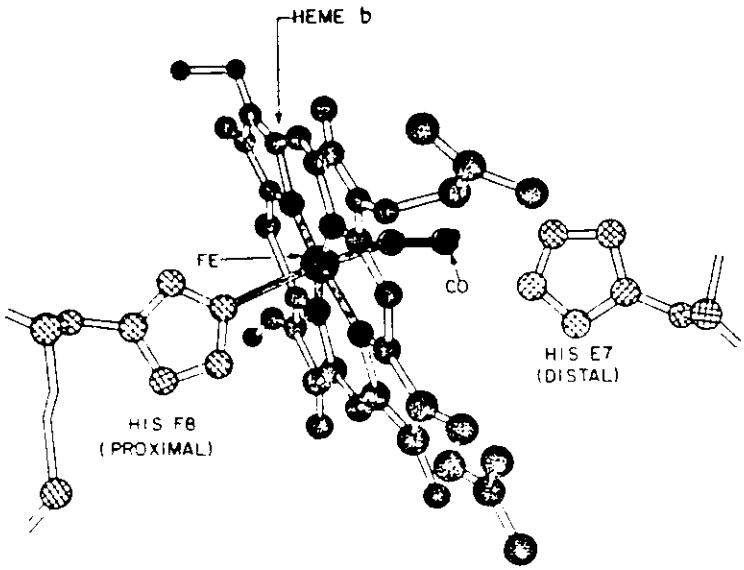

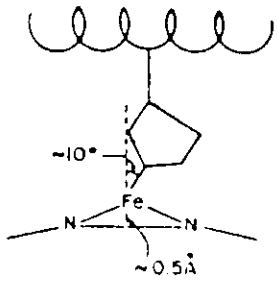

DEOXY HEME

5-COORDINATE
NON-PLANAR
HIGH SPIN (S=2)

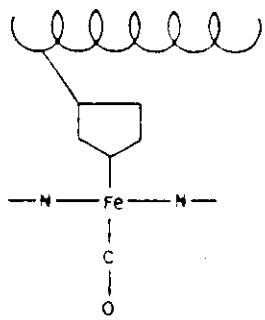

CO-BOUND HEME

6-COORDINATE
PLANAR
LOW SPIN (S=0)

Comparison of NM and HH myoglobins in the deoxy form ⇒

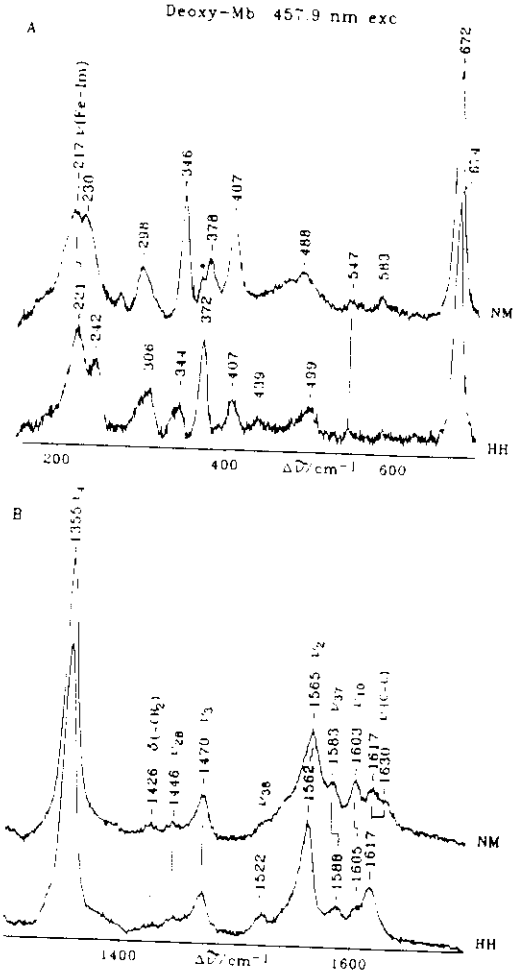

FIGURE 1: Resonance Raman spectra of deoxy forms of *Nassa mutabilis* (NM) and horse heart (HH) myoglobins, obtained with 457.9 nm excitation wavelength. Panel A shows the low-frequency region, and panel B shows the high-frequency region. Experimental conditions: 40 mW laser power at the sample; 5 cm^{-1} resolution; and 5 s/cm collection interval. The asterisk indicates a plasma line.

In NM → 217 cm^{-1} (Fe- Im stretch) lower than for HH → weaker bond strength → lower affinity for O_2 binding (expected for a cooperative process)

υ_2, υ_3, υ_{10} → bands characteristic of a 5-coordinate high spin heme (also for HH)

$\upsilon_{C=C}$ → 2 bands (only one for HH): due to interaction with the protein and/or differences in the two homodimers

Comparison of NM in the deoxy, oxy and met forms ⇒

Table 1: Resonance Raman Frequencies (cm^{-1}) of Deoxy-, Oxy-, and Met-Mb from *Nassa mutabilis*

mode	deoxy 5-c hs[a]	oxy 6-c ls[a]	met 6-c ls[a]
$\nu_{C=C}$	1630	1630	1630
$\nu_{C=C}$	1617	1620	1621
ν_{10}	1603	1638	1639
ν_{37}	1583	1604	1601
ν_{2}	1565	1581	1578
ν_{19}	1556	1594	1586
ν_{11}	1543	1563	1561
ν_{38}	1525	1547	1550
ν_{3}	1470	1503	1505
ν_{28}	1446		
δ_{CH_3}	1426	1429	1431
ν_{4}	1355	1375	1373
ν_{Fe-Im}	217		
ν_{Fe-O_2}		571	
ν_{CO}	1947		
ν_{Fe-CO}	517		
δ_{Fe-CO}	580		

[a] 5-c hs, 6-c hs, and 6-c ls, 5-coordinate high-spin, 6-coordinate high-spin, and 6-coordinate low-spin heme, respectively

Photolysis ⇒

571 cm^{-1} → Fe^{II} - O_2 stretch

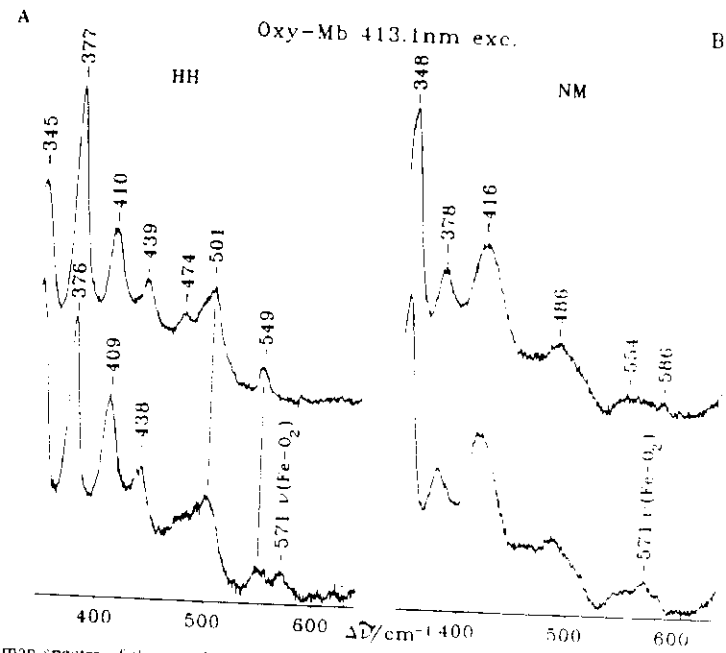

FIGURE 4: Resonance Raman spectra of the oxy forms of *Nassa mutabilis* (NM) and horse heart (HH) myoglobins in the low-frequency region, obtained with 413.1 nm excitation. Experimental conditions: 5 cm^{-1} resolution; (A) bottom spectrum obtained using a cylindrical lens, 8 mW laser power at the sample, and 24 s/cm^{-1} collection interval; top spectrum, 30 mW laser power at the sample and 6 s/cm^{-1} collection interval; (B) bottom spectrum obtained using a cylindrical lens, 8 mW laser power at the sample, and 24 s/cm^{-1} collection interval; top spectrum, 20 mW laser power at the sample, and 10 s/cm^{-1} collection interval.

Raman Study of Membranes from Torpedo marmorata (fish)

D. Aslanian, P. Grof, J-L. Galzi & J-P. Changeau

Biochim. Biophys. Acta 1148, 291 (1993)

Study of:

acetylcholine receptor structure

interaction with carbamylcholine and (+)-tubocurarine

Sample:

membrane fragments from the electric organ of T.m.

↓

rich in acetylcholine receptor (AcChR)

↓

ion channel composed of 4 classes of subunits $\alpha_2\beta\gamma\delta$

forms a transmembrane pentamer

Contains binding sites for cholinergic ligands

↓

carbamylcholine - binds to 2 sites/receptor molecule
activates ion flux through channel

(+)-tubocurarine - binds to the same 2 sites
inhibit action of activator

Sample:

8-10 mg protein/ml in Tris-HCl buffer (pH 7.5), 10°C

Excitation:

514.5 nm, 130 mW

- Secondary structure of AcChR from Amide I region ⇒
  - -buffer, lipid and aromatic amino acid vibrations were subtracted
  - - deconvolution
- - fitting with a linear combination of amide I spectra of standard proteins

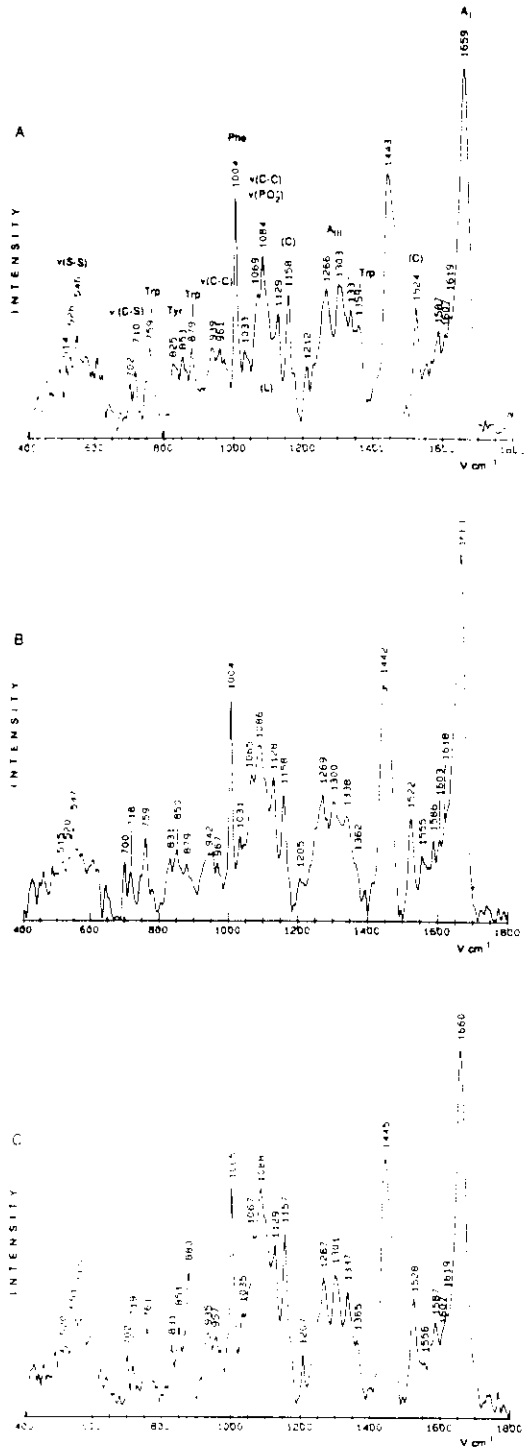

Fig. 1. (A) Raman spectrum of AcChR-rich membrane fragments from *T. marmorata* in 10 mM Tris-HCl (pH 7.5), 3 mM EDTA, 1 mM EGTA, after water and fluorescence subtraction. (B) Raman spectrum of AcChR-rich membrane fragments from *T. marmorata* in the presence of the agonist carbamylcholine (recording conditions as in A). (C) Raman spectrum of AcChR-rich membrane fragments from *T. marmorata* with AcChR exposed to the competitive antagonist (+)-tubocurarine (recording conditions as in A).

TABLE I

Secondary structure estimation of the AcChR-rich membrane fragments of T. marmorata electric organ

	Structure (%)			
	α_t (α_o α_d)	β_t (β_{ap} β_p)	T	U
Native membrane-bound AcChR	47 (29 18)	25 (24 1)	18	11
AcChR-carbamylcholine complex	48 (35 13)	25 (24 1)	18	10
AcChR-(+)-tubocurarine complex	39 (21 17)	26 (20 6)	25	13

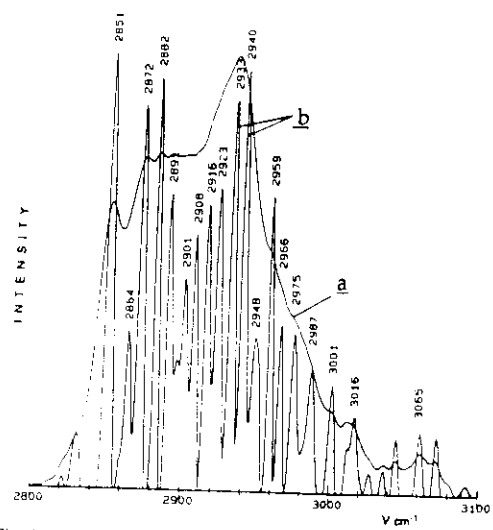

Fig. 4. Raman spectra of AcChR-rich membrane fragments from *T. marmorata* in the (C-H)-stretching region (recording conditions as in Fig. 1A): (a) experimental spectrum; (b) deconvoluted spectrum.

- Tyr doublet

$\frac{I_{850}}{I_{830}}$ { > 1.3 – tyr exposed to solvent (strong H bond acceptor)
< 0.9 – tyr buried (strong H bond donor)
0.9 → 1.3 - moderate H bonding

For the 3 samples ratio ≈ 1.2 → tyr mostly in hydrophilic regions

- Trp bands

≈ 1360 cm^{-1} sharp band- buried residue
intensity decreases if it becomes accessible to water molecules

AcChR + activator → trp exposed to aqueous medium
AcChR and AcChR + inhibitor → trp partly buried and partly exposed (well separated peak, but not very strong)

≈ 880 cm^{-1} - intensity decreases when residue becomes exposed

AcChR + activator → trp exposed to aqueous medium
AcChR → trp less exposed
AcChR + inhibitor → more buried

- S-S stretching bands

≈ 510 cm^{-1} → gauche-gauche-gauche configuration
≈ 525 cm^{-1} → trans-gauche-gauche configuration
≈ 540 cm^{-1} → trans-gauche-trans configuration

For AcChR and AcChr + activator → bands are at same positions
For AcChR + inhibitor → bands are at 520, 551 and 565 cm^{-1} → conformational changes in geometry of S-S bond

- C-H stretching
  2800-3120 cm^{-1} (lipid and protein contributions)

lipid:
  $\approx$ 2850 cm^{-1} symmetric CH_2 stretch
  $\approx$ 2880 cm^{-1} asymmetric CH_2 stretch (subtract contribution from protein)

$\frac{I_{2880}}{I_{2850}}$ - order parameter $\Rightarrow$ higher ratio $\rightarrow$ more ordered conformation

Observed: lipid fluidity decreases in presence of activator and in the presence of inhibitor

- C-C stretching
  1130 cm^{-1} and 1064 cm^{-1} $\rightarrow$ modes of all-trans conformers
  1090 cm^{-1} $\rightarrow$ modes of gauche conformers

In ordered lipid chain state $\Rightarrow$ all-trans bands are intense
In disordered lipid chain state $\Rightarrow$ gauche band is intense

Observed:
- Native: strong signal at 1084 cm^{-1} and shoulders at 1069 and 1129 cm^{-1} $\rightarrow$ disordered state
- With activator and with inhibitor: strong signal at 1086 and 1088 cm^{-1}, respectively $\rightarrow$ also disordered

Raman Study of Protein Aprotinin

S.E.M. Coalianni, J. Aubard, A.H. Hansen & O.F. Nielsen

Vibrational Spectroscopy 9, 111 (1995)

Studies:

- Secondary structure (amide I and III bands)
- Conformation around sulfur bridge
- Environment of Tyr

Aprotinin - synthetic form of basic pancreatic trypsin inhibitor
(58 amino acids, 3 S-S, 4 tyr)

Excitation: 1064 nm, 300 mW

Amide I study → sample in D_2O (to avoid water bending vibrations)

Amide III study → sample in H_2O

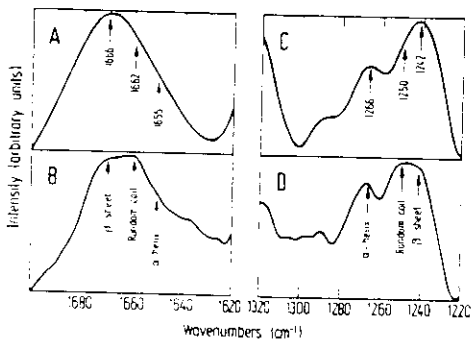

Fig. 3. The amide I region of NIR-FT-Raman spectra of (A) aprotinin powder and (B) a 20% (w/w) deuterium oxide solution in a windowless cell, and the amide III region of NIR-FT-Raman spectra of (C) aprotinin powder and (D) a 20% (w/w) aqueous solution in a windowless cell. Bands characteristic of specific secondary amide structures are marked with arrows.

Powder →
- predominance β-sheet
- some α-helix
- some random coil

In solution →
- higher content of:
  - random coil and
  - α-helix

Conformation around sulfur bridge & Environment of Tyr

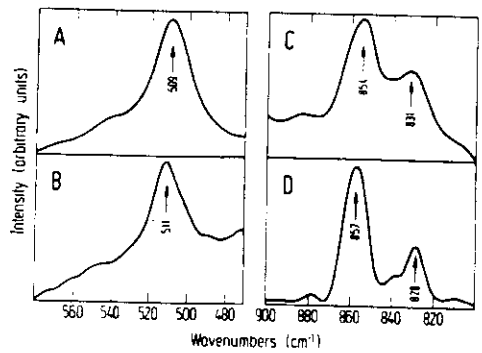

Fig. 4. (A) and (C) show NIR-FT-Raman spectra of aprotinin powder, and (B) and (D) show a 20% (w/w) aprotinin aqueous solution in a windowless cell. The band in A and B is characteristic of the sulfur bridge conformations and the doublet around 800 cm^{-1} to the hydrogen bonding of tyrosine.

- Sulfur bridge band around 510 cm^{-1} → 3 S-S bonds are in gauche-gauche-gauche conformation (for powder and solution)

- Tyr doublet → environment of tyr

$\frac{I_{850}}{I_{830}} > 1.25$ → all tyr are exposed to solvent (for powder and solution)

However from x-ray diffraction → 2 tyr are buried